Railway Right of Way Monitoring and Early Warning System (RailMEWS) Based on Satellite and Aerial Imagery

Final Report

by
Dr. Dimitris C. Rizos
Email: rizos@engr.sc.edu
Department of Civil and Environmental Engineering
University of South Carolina

Dr. Robert L. Mullen
Email: rlm@sc.edu
Department of Civil and Environmental Engineering
University of South Carolina

Sumanth V. Byrraju
Email: sbyrraju@email.sc.edu
Department of Civil and Environmental Engineering
University of South Carolina

April 2019

Center for Connected Multimodal Mobility (C^2M^2)

CLEMSON UNIVERSITY

Benedict College | The Citadel, The Military College of South Carolina | SC State University | University of South Carolina

200 Lowry Hall, Clemson University

Clemson, SC 29634

DISCLAIMER

The contents of this report reflect the views of the authors, who are responsible for the facts and the accuracy of the information presented herein. This document is disseminated in the interest of information exchange. The report is funded, partially or entirely, by the Center for Connected Multimodal Mobility (C^2M^2) (Tier 1 University Transportation Center) Grant, which is headquartered at Clemson University, Clemson, South Carolina, USA, from the U.S. Department of Transportation's University Transportation Centers Program. However, the U.S. Government assumes no liability for the contents or use thereof.

Non-exclusive rights are retained by the U.S. DOT.

Technical Report Documentation Page

1. Report No.	2. Government Accession No.	3. Recipient's Catalog No.

4. Title and Subtitle	5. Report Date
Railway Right of Way Monitoring and Early Warning System (RailMEWS) Based on Satellite and Aerial Imagery.	April 2019
	6. Performing Organization Code

7. Author(s)	8. Performing Organization Report No.
Dimitris C. Rizos, PhD. ORCID: 0000-0001-5764-7911 Dr. Robert L. Mullen, PhD. ORCID: 0000-0002-4321-5939 Mr. Sumanth Byrraju ORCID: 0000-0002-5633-9746	

9. Performing Organization Name and Address	10. Work Unit No.
University of South Carolina Dept. of Civil & Environmental Engineering 300 Main Str. Columbia, SC 29208 USA	11. Contract or Grant No. Contract # 69A3551747117

12. Sponsoring Agency Name and Address	13. Type of Report and Period Covered
Center for Connected Multimodal Mobility (C^2M^2) Clemson University 200 Lowry Hall, Clemson Clemson, SC 29634	Final Report 09/20/2017-10/09/2018
	14. Sponsoring Agency Code

15. Supplementary Notes

Conducted in cooperation with the U.S. Department of Transportation, Federal Highway Administration

16. Abstract

This report presents the findings of one-year study that explores the feasibility to use commercially available satellite and other aerial imagery to monitor the right of way of railroads for effects and conditions that could potentially trigger landslides and other geotechnical failures. Two major objectives have been identified: (1) Establish the methodologies for processing satellite and aerial images suitable for detecting and quantifying deformations on the right of way of railways at desired levels of accuracy; and (2) Provide recommendations for the development of a remote monitoring system. An extensive review of existing methods is conducted. Showcase studies have demonstrated that the current satellite technology makes it feasible to monitor the railway infrastructure for large- and small-scale deformations and changes in the ground moisture content with adequate resolution. The satellite analysis results can be superimposed to aerial visual imagery for ease of visual inspection and evaluation. Future work for the development of a monitoring system of the railway right of way needs to focus on verifying the accuracy of the techniques with in-situ measurements through conventional means and quantifying the changes of the moisture content.

17. Keywords	18. Distribution Statement
Satellite Imaging, DInSAR, PSInSAR, Railway Monitoring, Landslide Monitoring	No restrictions. This document is available through the National Technical Information Service, Springfield, VA 22161.

19. Security Classif. (of this report)	20. Security Classif. (of this page)	21. No. of Pages	22. Price
Unclassified	Unclassified	57	NA

TABLE OF CONTENTS

LIST OF TABLES

LIST OF FIGURES

EXECUTIVE SUMMARY

This report presents the findings of a one-year study that explores the feasibility to use commercially available satellite and other aerial imagery to monitor the right of way of railroads for effects and conditions that could potentially trigger landslides and other geotechnical failures. Two major objectives have been identified: (1) Establish the methodologies for processing satellite and aerial images suitable for detecting and quantifying deformations on the right of way of railways at desired levels of accuracy; and (2) Provide recommendations for the development of a remote monitoring system. In view of the objectives, satellite imagery in the radar frequency range of the electromagnetic spectrum has been obtained for locations around the world. The satellite data is available in the public domain. The Synthetic Aperture Radar (SAR) family of methods has been considered for the processing of the satellite data. Open source software for the implementation of these methods is available in the public domain. Two main methods are evaluated, i.e., the Differential SAR Interferometry (DInSAR) and the Persistent Scatterer Interferometric SAR (PDInSAR). Three showcase studies are presented in this report. The first two studies demonstrate the DInSAR technique as applies to detection of large scale ground movement observed as a result of a volcano eruption and a landslide. It is demonstrated that in addition to the ground movement in the case of a landslide, changes in the ground moisture content can be detected before the ground movement takes place. The third case study pertains to monitoring railway tracks for small scale movement at the Transportation Technology Center using the PSInSAR technique. PInSAR technique can detect small scale ground movement at discrete points on the earth's surface with resolution in the order of a millimeter. In all cases, it is demonstrated that the analysis results can be superimposed to aerial visual imagery for ease of visual inspection and evaluation. It is concluded that the current satellite technology makes it feasible to monitor the railway infrastructure for large- and small-scale deformations and changes in the ground moisture content in adequate resolution. Future work for the development of a monitoring system of the railway right of way needs to focus on verifying the accuracy of the techniques with in-situ measurements through conventional means and quantifying the changes of the moisture content.

CHAPTER 1

Introduction

1.1 Problem Statement

Infrastructure inspection, assessment, and maintenance are integral parts of the freight and passenger railway industry. Irregularities, damage and/or failure of the railway infrastructure and its components along the railway right of way disrupts service and productivity, impacts safety of operations and have adverse effects on the communities leading potentially to substantial economic loss and loss of life. Defects are caused by train operations, ageing, and/or acts of nature (e.g. landslides, earthquakes) and are manifested in the form of geometry changes of the right of way, e.g. ground movement, track settlement, loss of alignment and stability, and differential settlements at interfaces of rapid stiffness change, among others.

Landslides account for the majority of worldwide geologic hazards and cause significant loss of life and billions of dollars in damages (Figure 1).

Photo Credits:
(a) https://www.thehindu.com/news/national/karnataka/6ev9i4/article24747078.ece/alternates/FREE_660/21BGDUDHSAGAR;
(b) https://www.google.com/search?q=landslide+in+railway&rlz=1C1GCEA_enUS811US811&tbm=isch&source=iu&ictx=1&fir=SuOiNXDyJ3a-UM%252CFUTle6-GD7IRAM%252C_&usg=AI4_-kT5SToyBpl3GxGDl2SKQ1yk9K1Y7g&sa=X&ved=2ahUKEwj5vPuqw8DfAhVQm-AKHbIzBHcQ_h0wFnoECAYQCA&biw=1450&bih=564#imgrc=fvMVRvtv2sFLGM:
(c) https://www.railway-technology.com/features/featuretrain-has-been-cancelled-flooded-tracks-weather/attachment/featuretrain-has-been-cancelled-flooded-tracks-weather-2/

Figure 1: Rail Infrastructure Damage and Disruption of Service due to Landslides

It is estimated that in the US alone the death toll is 25 to 50 people and the damage is in excess of $2 billion annually. Railways cross areas of various geotechnical conditions, with a wide range of climates and local seismicity that may produce earth movement and geotechnical failures. Such events have detrimental effects on rail operations and safety and result in substantial economic losses. "*Barcelona train crash: At least one dead and dozens injured as landslide causes derailment in Spain"* (11/2018) (Embury-Dennis, 2018); "*Amtrak passenger train derails in Vermont; 6 riders injured*" (Fantz & Capelouto, 2015); "*Rock slide near Bonners Ferry shuts down BNSF track*" (11/2014) (The Spokesman-Review, 2014); "*Mount Washington landslide halts trains*" (4/2014) (Pittsburgh Post Gazette, 2014) are typical headlines for events related to natural earth movement that cause rail infrastructure damage, derailments and disruption of service. Derailments due to earth movement and geotechnical failure occur due to: 1) Fill failure; 2) Rockfall or rockslide in rock cut slope failure; 3) Track blockage by landslides originating outside of the railroad right of way, and 4) Track-bed failure by landslide or settlement in the ground beneath the track. Occurrence of landslides is due to two factors

(Dai, et al., 2002): 1) Triggering processes which initiate slope failures, i.e., hydro-meteorological conditions, earthquakes, etc; and 2) Regional factors that make a site susceptible to earth movement, i.e. geology and material characteristics (e.g. types and properties of soils, saturation, porosity), topography (e.g. slopes, vegetation), human intervention (e.g. land use, irrigation) and other physical factors.

Geometry changes of the right of way caused by train operations and aging are typically smaller in magnitude and evolve at a slow rate over time compared to changes caused by acts of nature that can be of large amplitude and take place within a short period of time. However, acts of nature events are often preceded by small scale geometry changes that can take place over a period of weeks or even months before the event. In both cases the exact location of the defects is not known a-priori.

Conventional methods for monitoring and inspection of the railway infrastructure use in-situ measurement practices (e.g. GPS, surveying and visual inspections) or video and measurement systems mounted on dedicated track inspection vehicles and can potentially disrupt operations. The frequency of deployment of conventional inspection and monitoring methods is relatively low due to the high cost associated with such operations and do not provide network wide monitoring. They typically do not monitor the rate of change of monitored parameters over time and, therefore, are not predictive in nature by themselves. Prediction of landslides, on the other hand, is not trivial and not reliable with established technologies. Traditional mapping and monitoring through instrumentation are either not possible because of the lack of scientific expertise and prohibitive budgets or not practical since it is limited to rather small areas, often with difficult site accessibility, obstructed visibility, and high terrain complexity. Early detection and improved prediction of the true risk potential for landslides and/or geotechnical failure is now feasible due to the advent of affordable satellite imagery coupled with recent advances in remote sensing, data collection, and image analysis algorithms.

1.2 Objectives of this report

This report presents the findings of a one-year study that explores the feasibility to use commercially available satellite and other aerial imagery to monitor the right of way of railroads for effects and conditions that could potentially trigger landslides and other geotechnical failures. Two major objectives have been identified: (1) Establish the methodologies for processing satellite and aerial images suitable for detecting and quantifying deformations on the right of way of railways at desired levels of accuracy; and (2) Provide recommendations for the development of a remote monitoring system. This report is organized as follows: Chapter 2 presents the fundamentals and background on remote sensing. Chapters 3 discusses the InSAR family of techniques for detecting ground motion and landslide recognitions from satellite imagery. Chapter 4 and 5 focus on the DInSAR and PSInSAR techniques and present the implementation of the methods for detecting surface movement. Chapters 6 and 7 present showcase studies that demonstrate the feasibility of implementing satellite image processing for the detection of large scale (e.g. landslides) and small scale (subsistence) surface deformations. Chapter 8 presents the conclusions of this feasibility study.

CHAPTER 2

Remote Sensing Fundamentals and Background

Remote sensing in its most basic form can be described as observing or collecting data from a monitoring target without having any contact with it. Remote sensing techniques are using devices (sensors) that observe the interaction between the electromagnetic spectrum with matter. Landslide investigation in the past few decades always used some form of remote sensing techniques. In this chapter, most of the remote sensing techniques and sensors are briefly explained. It is important to integrate these techniques for landslide investigation as they would reduce the cost of manpower and it's easy to make early predictions with them and hence help in mitigating the damage caused by them (Scaioni, et al., 2014). Landslide investigation activities are usually performed in two steps, i.e., landslide recognition and landslide monitoring. Landslide recognition is the initial step and is generally followed by landslide monitoring and hazard analysis.

2.1 Electromagnetic spectrum

Electromagnetic (EM) spectrum is the entire range of energies that are produced as a result of interaction between matter and energy. The different regions of the EM spectrum are distinguished with respect to the wavelength to: gamma rays, X-rays, ultraviolet rays, visible light, infrared rays, radar, FM, TV, shortwave and AM as illustrated in Figure 2.

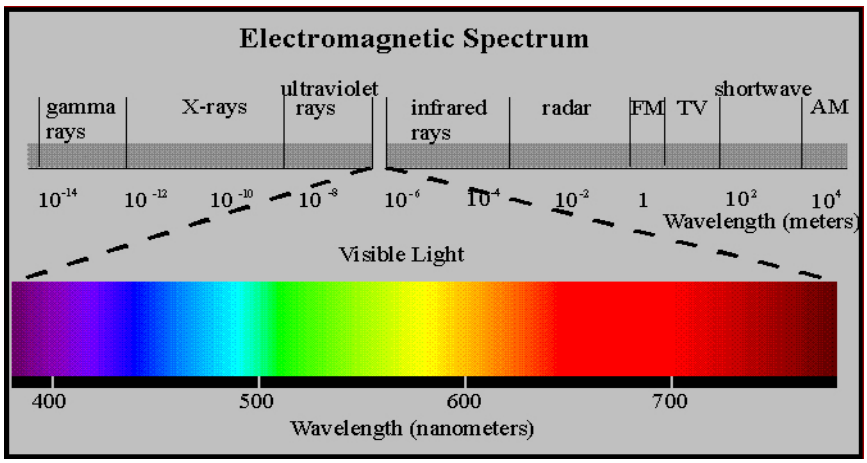

Figure 2: The Electromagnetic (EM) Spectrum

The interaction of the energy carried in EM waves with an object produced one or more of the following effects:

Wave Absorption: This is the portion of the incident energy that is converted to internal energy in the object.

Wave Scattering: This is the portion of the incident wave that upon contact with the matter bounces off the object and propagates in multiple directions.

Wave Emission: This is the energy emitted by the matter when its atoms fall from a higher excited state.

Wave Transmission: This is the energy that travels through the matter without affecting it in any way.

When the incident wave energy is emitted by the sun, and in view of the aforementioned effects, the different regions of the EM spectrum interact with the earth as follows: The Gamma and X rays are entirely absorbed by earth's atmosphere. The part of the Ultraviolet rays (UV) in the wavelength range 0.03 – 0.4 micrometers is completely absorbed by the ozone layer. The remaining UV part in the wavelength range 0.3-0.4 μm is invisible to the naked eye and behaves similar to visible light. Different parts of the visible light are reflected by matter and the color of the matter as seen by the naked eye is the reflected part of the light. The infrared rays are absorbed by matter as heat transfer. The radar waves in the wavelength range 0.1-100 cm are absorbed by the atmosphere, while the rest are transmitted through the atmosphere. The interaction of the EM spectrum with the atmosphere is depicted graphically in Figure 3.

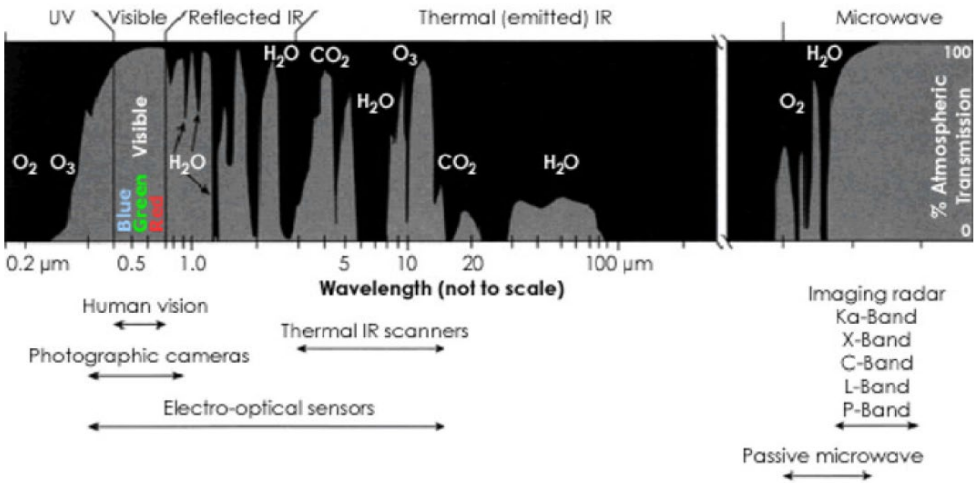

Figure 3: Interaction of wavelengths of EM spectrum with water, oxygen and ozone major components of the atmosphere (Clark & Rilee, 2010)

2.2 Optical Sensors

In the field, optical sensors capture the interaction of EM waves with matter. These sensors can be divided into two types based on the origin of the energy source. If the source of the energy is not natural, e.g. an instrument generates the energy, then it is called an active sensor. If the source of energy is natural, e.g. the energy is emitted by the sun or the target then this type of sensor is called a passive sensor. Most of the sensors observe the light interactions that are not visible to the naked human eye and the observations are developed in false color composites, so scientists can observe the necessary data. Furthermore, depending on the mounting platform's sensors are classified into ground-based, airborne and space-borne. The following sensors are used in landslide and ground movement investigation. They are described based on the type of sensor and the EM spectrum range they detect.

2.2.1 HR/VHR

High-Resolution (HR) and Very High-Resolution (VHR) images are acquired by passive sensors which observe visible light and have a resolution of 30 meters and 60 centimeters, respectively. They are available onboard the *Landsat* and the *QuickBird* satellites (Munzer, 2010).

2.2.2 Panchromatic images

Panchromatic images are in black and white but represent all the wavelength of visible light. These sensors are passive and have higher resolution compared to their counterparts in the visible spectrum (CRISP, 2017).

2.2.3 Multispectral

Multispectral image contains the properties of the target beyond the visual spectrum, like Infrared (IR) and Ultraviolet (UV) waves. These are observed by sensors which use additional filters and therefore are considered passive sensors. The resolution in these sensors differs from the visual spectrum as these images observe the absorption and transmission properties of the target (CRISP, 2017).

2.2.4 LIDAR

LIDAR is an acronym for Light Detection and Ranging sensors. These sensors use laser waves (wavelength of 1550nm) to illuminate the target and measure the reflected pulse. Since the source of the light is on the sensor platform these sensors are considered active sensors (GISGeography, 2017).

2.2.5 SAR

Synthetic Aperture Radar (SAR) sensors are similar to LIDAR sensors but they use radar waves (0.1-100cm) and cover a much larger area as compared to LIDAR. Since these sensors also include their own energy source they are considered active sensors.

2.3 Landslide Recognition

Landslide recognition involves all activities required to detect landslides in a specific region. These involve analyzing past events, building inventories, etc. This step does not involve the detection of a single landslide, but rather the mapping of the location of multiple landslides in each area. Most of the techniques that are described depend on the principle that landslide events cause a disturbance in the area. These changes can be detected by aerial or satellite images as there will be a change in the topography which can then be taken as a mark of slope instability. These techniques are considered novice or basic and are useful to find shallow landslides or instabilities, whereas much more complex methods are used for deep-seated landslides. Some of the sensors and techniques used in landslide recognition are also used in monitoring, however, the acquisition frequency and application differ. Landslide recognition is discussed next based on the technique used for detection rather than the sensor, as different sensors are used within the same technique.

2.3.1 Visual interpretation and geomorphic feature extraction

This is the most commonly used technique in landslide recognition due to the high-quality images that are obtained from High Resolution (HR) and Very High Resolution (VHR) sensors that can cover large areas. This interpretation technique is based on the concept that certain characteristic changes in a target location can be attributed to landslide activity. The sensors used in this technique mostly depend on the visible region of spectrum and photogrammetry. This technique is based on the fact that most landslides cause a topographical change which can be detected over a period of time. A sensor takes multiple images of the monitored location while a trained geomorphologist can detect a change in the images. This technique is effective when considering the satellite orbit as the images can be taken at required intervals and the detection of changes is more optimized (Fiorucci, et al., 2011). Figure 4 shows the application of this technique to detect landslides.

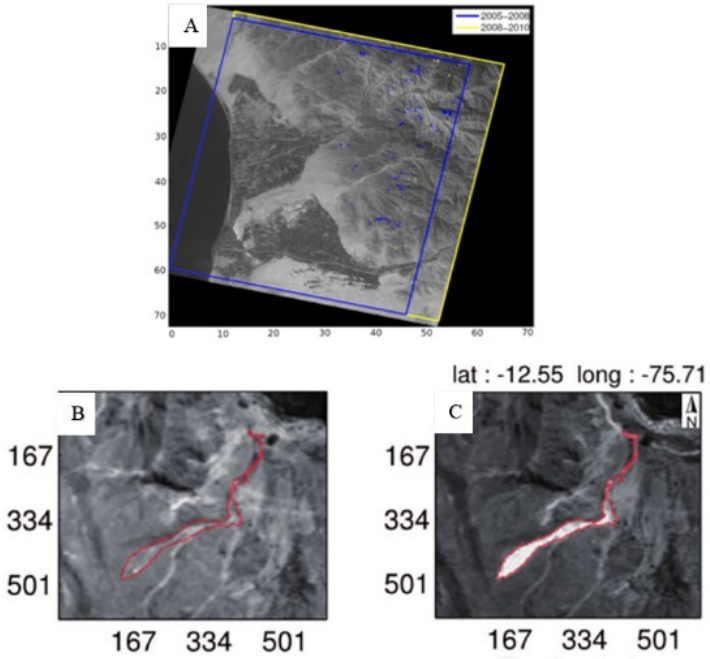

Figure 4: In image A, combination of visual interpretation and automatic pixel recognition methods are used to detect landslides. Images B and C show the landslide detected using the above method. Image B shows the location before the event and image C shows the landslide after the event (Lacroix, et al., 2013)

An application example is reported in (Fiorucci, et al., 2011). In this study the investigators resolved the problem of getting timely post-event aerial photographs by using HR and VHR optical images. The study area in this experiment is 90km^2 in central Italy, Umbria which has been experiencing high landslide activity. The study was performed using IKONOS satellite images along with *Terra Italy* aerial photographs. The investigators found a total of 161 landslides from IKONOS out of which 13 new landslides were not detected by *Terra Italy*. Some of the landslides detected are shown in Figure 5. The study concluded that visual interpretation of aerial and satellite image is more

accurate than preexisting reconnaissance inventory obtained through unsymmetrical field surveys.

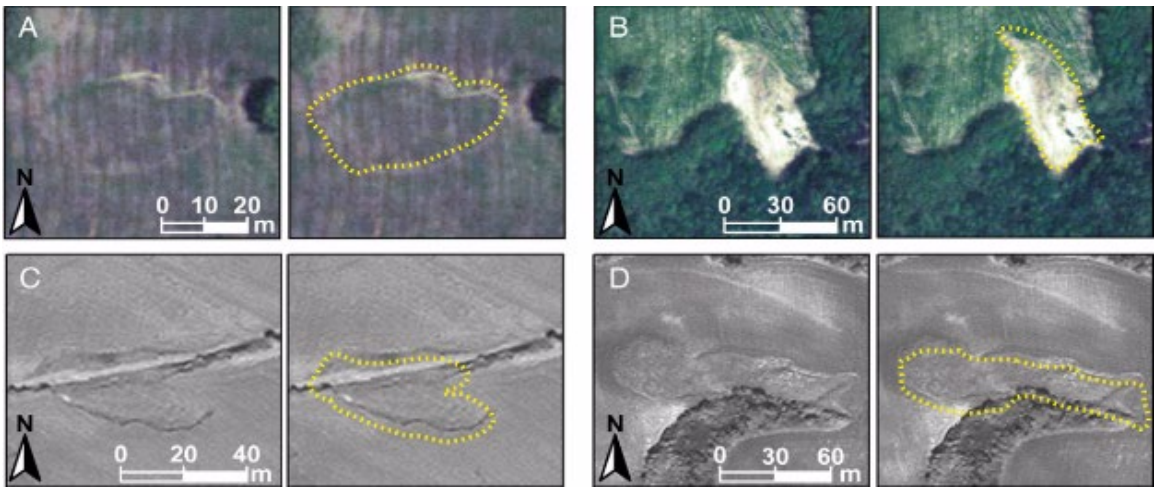

Figure 5: Images of landslides recognized by color ortho-photographs (A and B) and panchromatic images (C and D). The yellow lines highlight the detected landslide (Fiorucci, et al., 2011)

2.3.2 Image fusion technique

The images obtained from a satellite are improved by using the technique called image fusion. This is a technique in which two images are merged to obtain a better-quality image. This is extremely useful in landslide investigation as the image obtained from a satellite the first time may not have the needed accuracy to detect the change in topography. Image fusion techniques are not only used to improve the quality of the image but are also used to combine two images which have distinct spatial and spectral characteristics. The resulting hybrid image will have characteristics of both parent images. This technique is implemented because the image resolution changes for different spectral ranges, even though they are taken from the same satellite (Liu, 2000). Using image fusion, a high-quality panchromatic image can have additional spectral information imbued into it which can make the observation of landslides from these images easier. In Figure 6, HIS Image fusion technique (Marcellino, et al., 2009) is used to detect landslide.

An implementation example of the image fusion technique use reported in (Nichol & Wong, 2005). In this study a 36km^2 heavy landslide area on Lantau Island, Hong Kong was investigated. The investigators used automatic change detection technique to detect small landslide from medium resolution SPOT images and used image fusion technique for qualitative interpretation of landslides. Multispectral images of lower spatial resolution were fused with panchromatic images of higher spatial resolution. To achieve this effectively, four-image fusion techniques were used namely, the HIS method (Mathew, 1999),

Figure 6: In this image landslide were detected using IHS image fusion technique. (Marcellino, et al., 2009)

the Brovey transform method (Gillespie, et al., 1987), the smoothing filter modulation method (Liu, 2000) and pan sharpening (Zhang, 2002). From the methods tested the pan sharpening method was found to be most effective because the fused image from pan sharpening was the least spectrally degraded and it contained the maximum information. Figure 7 shows the landslide detection using image fusion technique with pan sharpening.

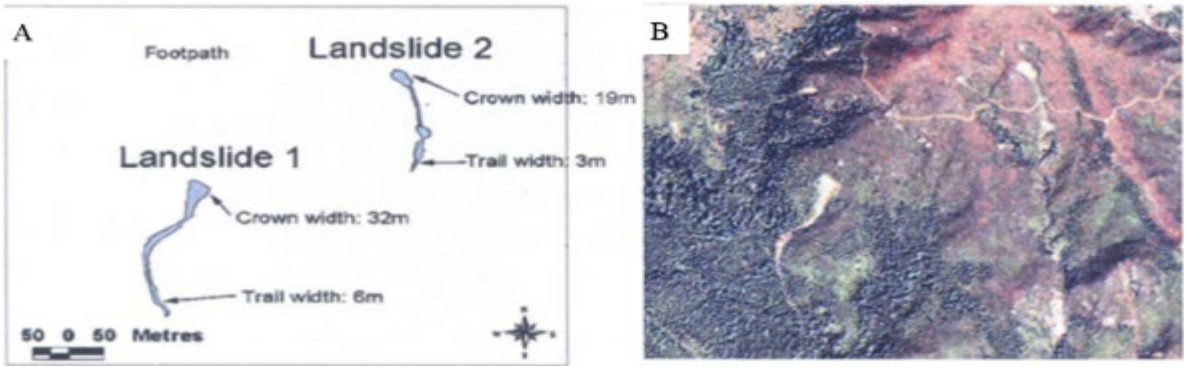

Figure 7: The above image (A) shows the detected landslides and the corresponding pan-sharpened fusion image (B) (Nichol & Wong, 2005)

2.3.3 Stereovision

Stereovision is a process of creating a three-dimensional (3D) image from two images taken at a certain distance from each other. This technique uses the same concept used by our eyes to create a 3D view. For landslide recognition two images are calibrated and are processed using a stereometric program to create a 3D image. This process is sometimes done using a special device from which a geomorphologist is capable of detecting landslide. The landslide generally looks like sliding of ground or flow pattern and can be seen in Figure 8 (Alkevli & Ercanoglu, 2011). It should be noted that detecting

landslides using this method depends on the experience and training of the geomorphologist and is unreliable as there does not exist any actual standards. But this technique does not require any sophisticated technical skills and is widely used. This is also due to the fact that recent advancements in computers have improved assisted stereovision (Haeberlin, et al., 2004).

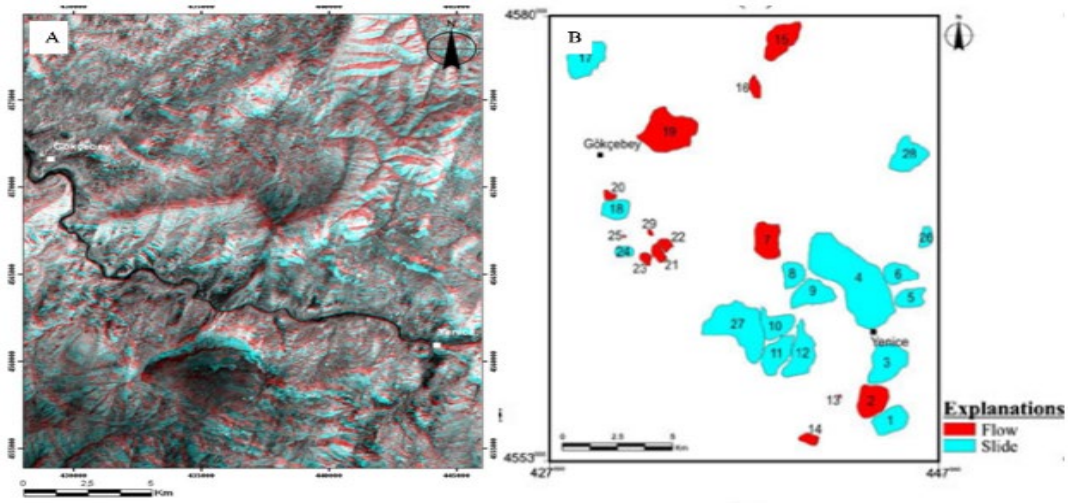

Figure 8: Image A represents the stereo image used to detect landslides. The landslides detected using image A are shown image B (Alkevli & Ercanoglu, 2011)

A case study is reported in (Murillo-Garcia, et al., 2015). This study area is in Puebla central Mexico, covers 54Km^2, and is mountainous terrain. The investigators performed visual analysis of stereoscopic pairs of VHR satellite images. Geo Eye-1 stereoscopic pair images with spatial resolution on panchromatic band were used. To improve the 3D models a computer software was used to assist in the identification of landslides. The investigators were able to detect 390 landslides using stereoscopy and additional landslides were later detected by field survey. Stereo mirror system and landslide detected are shown in Figure 9.

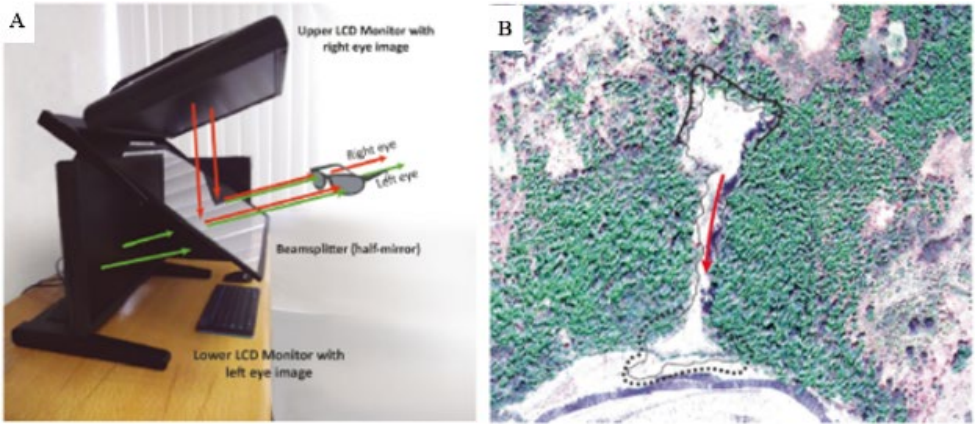

Figure 9: Stereovision case study: (A) The stereo mirror system; (B) the landslide Digital Elevation Model (DEM) from GeoEye-1 stereo pair (Murillo-Garcia, et al., 2015)

2.3.4 LIDAR

Light Detection And Ranging (LIDAR) is a remote sensing technology that uses light reflection to obtain the spatial coordinates of the target location. LIDAR systems exist in both terrestrial and airborne format but for landslide recognition, they are used on board an airplane or satellite. When the sensor flies over the location of interest the laser beam swipes the area. As the light is reflected to the sensor the distance between the sensor and the location is found through travel path and time analysis yielding a highly accurate image. The image is then processed and a Digital Elevation Model (DEM) is created for visualization and spatial analysis. From the DEM, a landslide can be detected by a geomorphologist or by assisting software. The landslide depicted in Figure 10 is obtained using a similar method. The additional benefit of using a LIDAR DEM is that the complete displacement field for the whole landslide is obtained as compared to point measurement (Jaboyedoff, et al., 2012). This process is better explained in the following example.

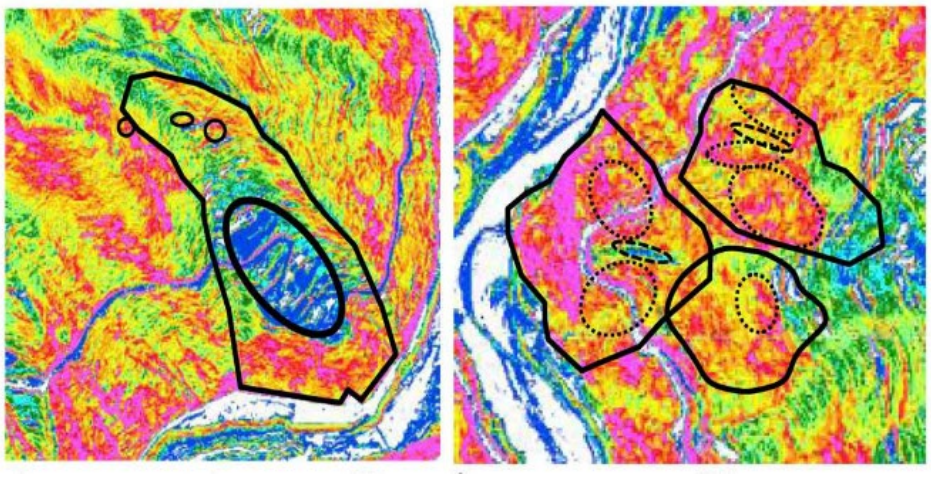

Figure 10: Deep seated landslides are detected from eigenvalue and slope filter ratio obtained from airborne LIDAR. The image above represents the spatial distribution of slope angle (Kasai, et al., 2009)

An example study is reported in (Chen, et al., 2014). The region is located near the Shazhenxi town in China and covers an area of 21.6Km^2. In this study, the LIDAR derived topographic images (Figure 11) were used along with field investigation and visual interpretation of aerial images. The study concluded that some new features can be extracted from LIDAR derived Digital Terrain Model (DTM) and proved that LIDAR is not affected by topographic shadowing which generally effects radar type images.

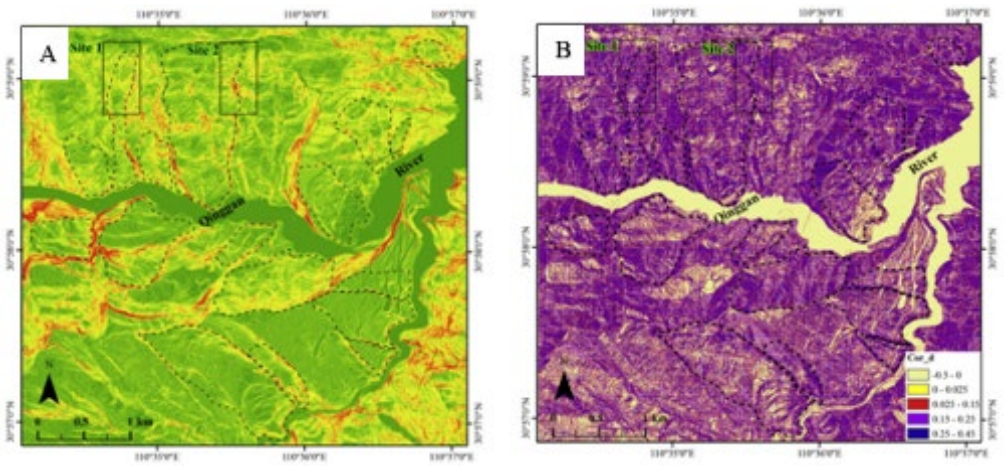

Figure 11: Image A shows the moving average filter map for slope and landslide. Image B shows the average correlation texture map for DTM and landslide locations. Landslides in both images are marked by dotted lines (Chen, et al., 2014)

2.3.5 Automatic landslide recognition

Automatic landslide recognition is not a new concept in landslide recognition but due to the possibilities of error, human oversight has been necessary. The technique is pixel based i.e. the computer program involved analyses each pixel from RS data and detects changes that are related to landslides. This method in most studies has been known to introduce numerous errors as seen in Figure 12 (Moine, M, et al., 2009).

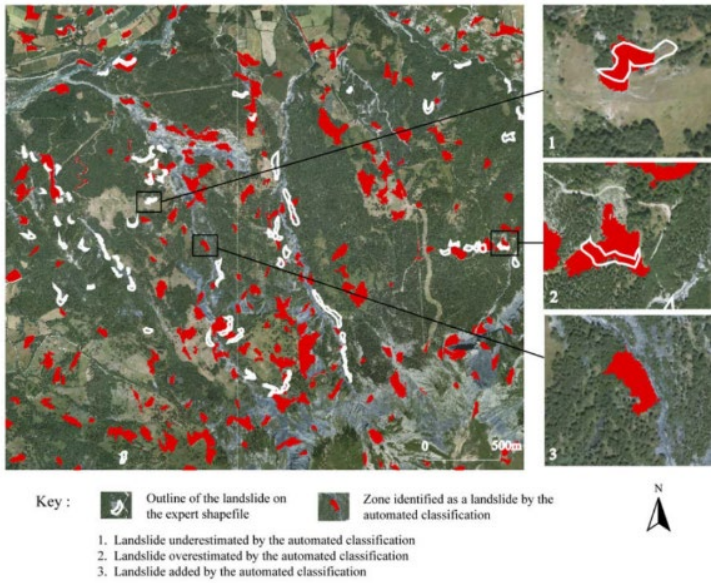

Figure 12: Landslides detected from semi-automatic landslide methods along with some false positives (Moine, M, et al., 2009)

New studies conducted in the past decade have taken a new approach in which the algorithm involved switched to object-based study instead of pixel-based study. This

improved the accuracy as the algorithm treats the landslide as an aggregation of pixels instead of spatially unrelated cells (Blaschke, 2010). This can be observed in the case study reported in (Lu, et al., 2011). This study was conducted in the Messina province of Sicily, southern Italy. The area was affected by intensive prolonged rainfall which triggered numerous landslides (shallow and debris flow). Two areas which were most damaged were surveyed for this study. Two Quickbird images with zero cloud cover were used. The landslides detected using the automatic approach were compared with manual landslide inventory. Their accuracy was compared on the number and spatial extent of mapped landslides. From the method used the automatic algorithm detected 242 landslides and manually 285 landslides were detected. This technique was proven to be effective with few false positives as exceptions as can been in Figure 13 where both the landslide and the false positives are highlighted.

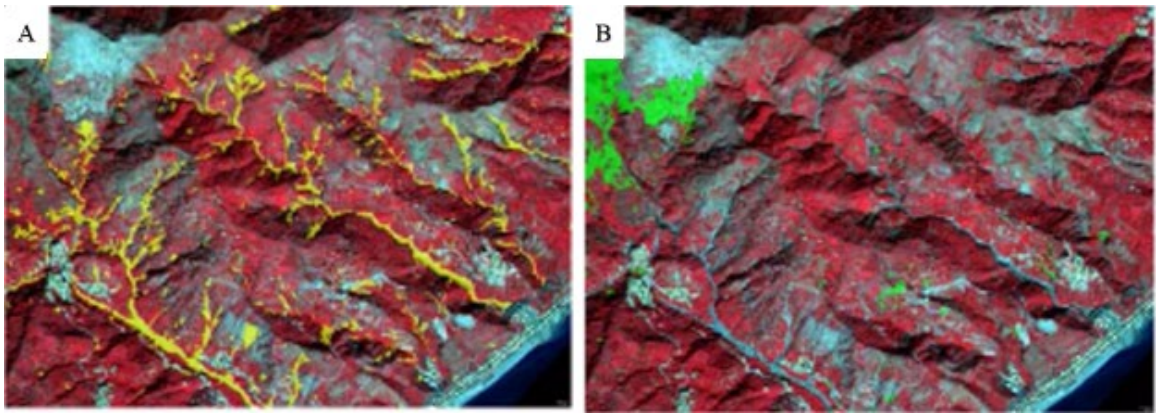

Figure 13: Image (A) shows the detected landslides (marked in yellow) using the automatic method. Image B shows the false positives obtained from this method marked in green (Lu, et al., 2011)

2.3.6 InSAR/DInSAR

Interferometric Synthetic Aperture Radar (InSAR) is a technique that uses SAR sensors to recognize landslides. A SAR sensor is an active microwave sensor which records the radar echo from the target location. The SAR sensor uses one of the three bands available, i.e., C, L, and X which have a wavelength of 5.6cm, 23.6cm and 3.1cm, respectively (Lillesand & Kiefer, 2008). InSAR technique detects landslides by calculating an interference pattern which is obtained from the phase difference between two SAR images at specified intervals. The phase difference contains possible ground displacement along with other “noise” which can be reduced, or eliminated if the coherence between the two images is high. Differential Interferometric Synthetic Aperture Radar (DInSAR) is an InSAR technique which removes topographic noise from two SAR images to extract the displacement pattern This is visible in Figure 14 (Guzzetti et al. 2009).

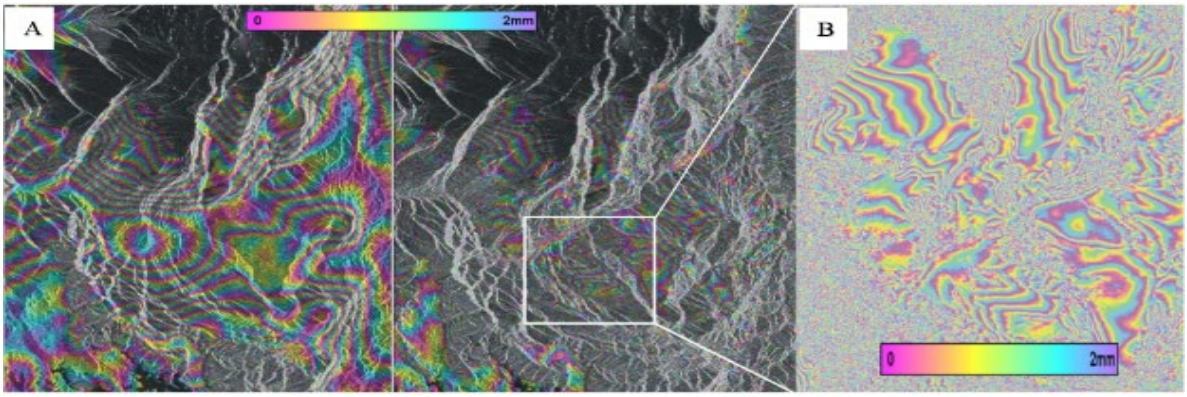

Figure 14: The above images represent the fringe pattern from InSAR. Picture A shows the two-pass processing and picture B shows the three-pass processing. The enlarged image in B represents movement rates around 14mm in 3 months (Riedel & Walther, 2008)

An example is reported in (Delacourt, et al., 2009). In this study was performed in La Reunion Island which is in the Indian Ocean which experiences constant slope movement and huge landslide activity due to climate and topography. The DInSAR analysis was carried out using Radarsat C-band images and Jers-1 L-band SAR images. From the research, it has been shown that the L-band SAR images have a prominent application in the future. It has also been stated that the lack of archive significantly reduces the effectiveness of such studies as more acquisitions improve the results. Results from C-band and L-band are shown in Figure 15.

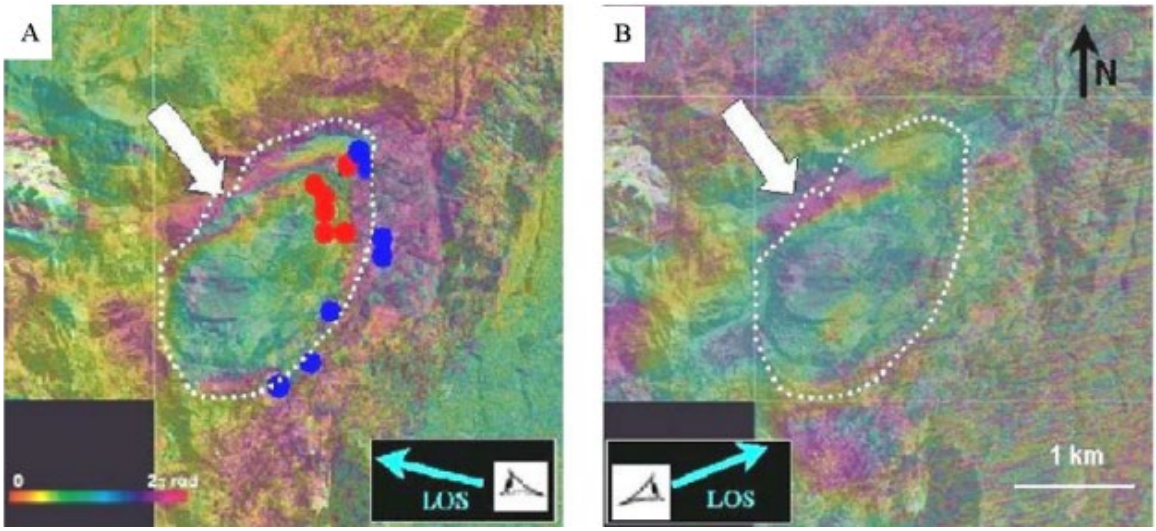

Figure 15: The above images represent the landslides detected from (A) C-band satellite and (B) L-band satellite. The arrow indicates the unstable area which is visible in both images (Delacourt, et al., 2009)

2.3.7 Thermal InfraRed

Out of all the techniques mentioned here, TIR is the least promising technique and can only be used in very rare cases. This is due to the constant change of temperature of the target location nearly every day due to weather, soil, climate, etc. Theoretically, the concept behind this method is that some landslide activity is directly related to soil moisture and saturation which is directly proportional to the temperature of the soil. The sensor calculates this, and landslide risk can be estimated. This technique has been successively used to map glacier-related landslides like rock and ice avalanches as changes in these types of landslides can be easily be detected from thermal sensors (Weng, 2009).

2.4 Landslide monitoring

Landslide recognition is just the first part of the investigation. These landslides must be observed over a period to observe their condition and to see if there is a potential to change. This change can be in their size or condition. This form of observation is called landslide monitoring. Landslide monitoring is handled through qualitative assessment of the general conditions of a landslide-prone slope a long time, or through the quantitative measurement of ground deformation and surface point displacements. Since most of the remote sensing sensors revisit at regular intervals observing these progressive deformations is ideal. The techniques in landslide monitoring are comparison-based studies and some of these techniques are automatic or semi-automatic and discussed next.

2.4.1 Digital Image Correlation

This is an advanced technique that uses a combination of other techniques to preprocess the images after which this technique is applied to monitor the target location. In a preprocessing phase, two stereoscopic images of the location are first obtained each with a time gap as large as of several years depending on the monitoring frequency. Both images must be taken from the same height. For successful correlation, the images must be of the same geometry and orthorectification to both images must be done, after which, the two DEMs are developed and Digital Image Correlation can now be conducted. Subsequently, to quantify the ground displacement a correlation window is defined to the oldest image, the size of which depends on the accuracy of the displacement required and the spatial resolution of the velocity field. This window is searched on the newest image to increase the correlation function. The ground displacement is the measure of shift between the 2 acquisitions by the pixel size (Travelletti, et al., 2012). This process is repeated for each pixel until the complete displacement field is obtained. This concept is demonstrated in (Delacourt, et al., 2004). In this study two aerial stereoscopic image pairs have been acquired over four years apart. The study area is in the French Southern Alps and covers 36 Km^2. The landslide investigated is called “La Clapiere”. The investigators applied optical correlation technique to derive deformation maps of landslides that have continuous deformations. This is seen in Figure 16. The study also concluded that the limitation of DInSAR can be overcome if used in combination with optical correlation.

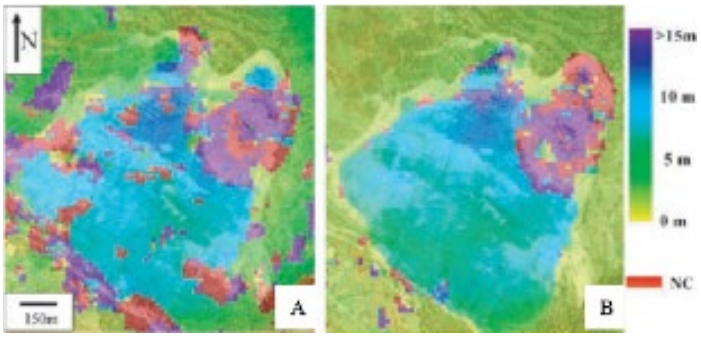

Figure 16: Displacement map obtained by correlation between aerial photographs. A 1999 to 2003 and B 1995 to 1999. NC from the scale represents no significant displacement because of poor correlation values (Delacourt, et al., 2004)

2.5 Comparison of HR-DEM

In this technique DEM are created from high-resolution images. The high-resolution images can be taken from satellite images or laser scanning techniques (Brückl, et al., 2006). In the case of a terrestrial laser, a station is built opposite the location to be monitored. Since the station can measure the reflection of light regularly, the landslide displacement is computed by comparing the DEM at regular intervals (Bitelli, et al., 2004). This technique is explained in the terrestrial laser scanning example reported in (Corsini, et al., 2009). In this study the Trafoi landslide in South Tyrol (Italy) is investigated. To obtain High Resolution DEM the investigators used LIDAR devices mounted on a Helicopter and the test area was surveyed three times between 2005-2007. The HR DEMs have been used to estimate surface roughness that helps in understanding the landslide internal activity. The researchers have concluded from this study that the comparison of multitemporal DEM was useful for calculating depletion and accumulation at the slope scale. Figure 17 shows landslide development and the outline of the landslide area when the area was investigated.

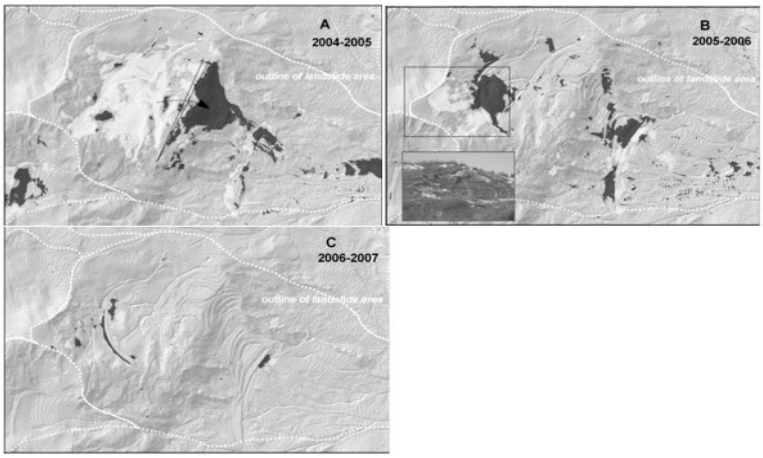

Figure 17: DEMs obtained from LiDAR datasets show the landslide. The dotted line points the outline and progression of landslide (Corsini, et al., 2009)

2.6 SAR Interferometry

2.6.1 Spaceborne

In the last two decades, advanced Differential Interferometric SAR (DInSAR) techniques have been successfully used to monitor slow-moving landslides. This is because large stacks of data are available as the satellites take images continuously at regular intervals as they follow their orbit. This process also improves the coherence between the images. The time period between each image depends on the user as the latest satellites have an orbit period of 2 days (Cosmo-sky med). The displacement that can be detected by this method is equal to 0.25 wavelength of SAR sensor. therefore, a sensor with X-band can observe a displacement of 8mm (Cascini, et al., 2010). An application example is reported in (Bianchini, et al., 2013). This study was conducted in the Tramuntana Range, Majorca (Spain). The investigators used PSInSAR to generate the Landslide activity map shown in Figure 18 (a). The acquisitions needed were taken from L band, ALOS sensor and a total of 14 number of acquisitions were performed. From the analysis, the investigators concluded that using L band SAR data detection of ground movement is faster as compared to the C band. Finally, the investigators were successfully able to monitor each landslide and assign its respective velocity. Figure 18 shows the landslide inventory maps being developed using PSInSAR and statistical evaluation of the database.

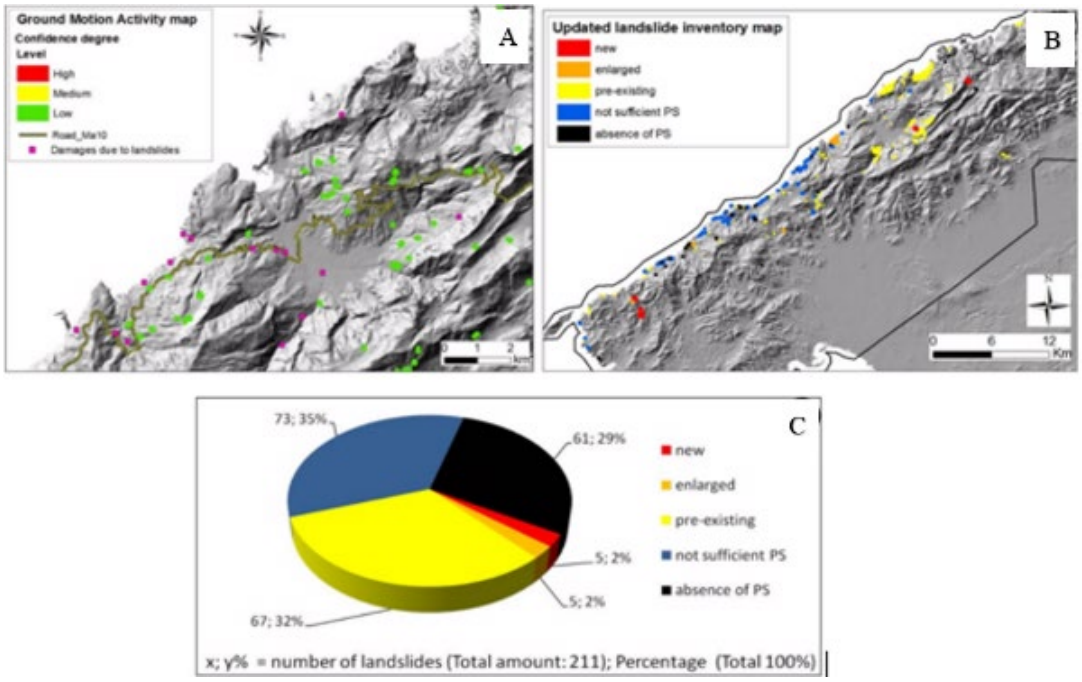

Figure 18: Ground motion activity detected by PSI (A). Landslide inventory map updated in Tramuntana Range (B). Statistical evaluation of landslide database improvement (C) (Bianchini, et al., 2013)

2.6.2 Terrestrial

Terrestrial Interferometric Synthetic Aperture Radar (TInSAR) is a ground-based radar technique that is used to monitoring displacements. TInSAR is performed by placing radar sensors on the rail and taking acquisitions of the target area from two different sensor locations. From the two acquisitions, interferometric techniques are applied to develop DEM and obtain displacement maps (Tarchi, et al., 2003). The accuracy in this method is greater than space-based interferometry as the signal to noise ratio is very high in this method due to a short baseline and short monitoring distance. This technique is not restricted to landslide investigation but also in the displacement analysis of man-made structures like buildings and roads (Mazzanti, et al., 2015). In this study, the landslide Tessina located in North Eastern Italian Alps was monitored using ground-based SAR system. The SAR installation (Figure 19 (A)) was used for early warning purpose as the landslide showed signs of being active again and it posed risk to nearby villages. The landslide was monitored using a portable SAR instrument. From the data that is obtained, the DInSAR technique (Figure 19 (C)) was used to monitor the landslide with millimeter accuracy. The data obtained is used to monitor the kinematic and short-term evolution of the landslide. The investigators concluded that ground-based SAR has numerous advantages to its space-based counterpart and further application is needed taking these advantages in mind. In Figure 19 the experimental set up of the TInSAR is shown along with the DEM generated by the machine.

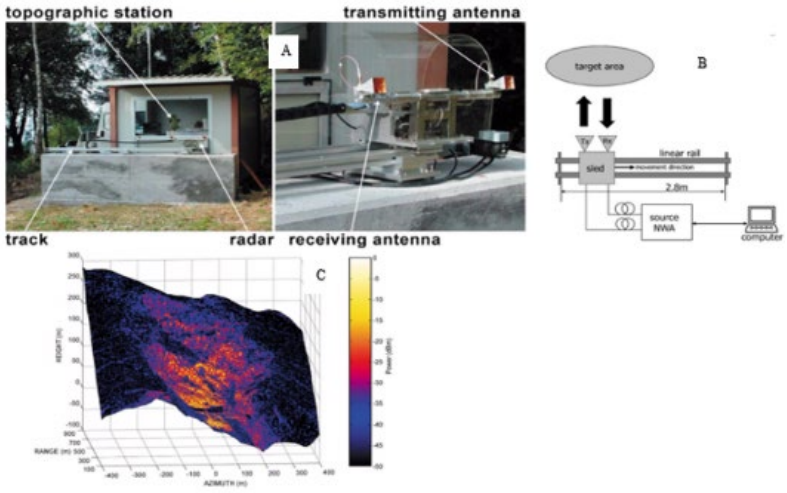

Figure 19: (A)represents the field set up of instrumentation (B) shows the technical scheme the equipment (C)shows the DEM of the target scene projected represented in local coordinate system with center being the point of origin (Tarchi, et al., 2003)

2.7 Techniques used for different types of landslides.

All the remote sensing techniques mentioned above cannot be used for each of the mentioned landslides because each has its own unique failure mechanism. Table 1 provides the technique used for some of the common types of landslides.

Table 1: Landslides and Remote Sensing techniques to investigate them

Land slide	R.S Technique	Platform	Investigation	Auto Process	Multi Techniques
Falls	Terrestrial Laser Scanning	Terrestrial	Recognition		
			Monitoring		
	Thermal Infra-Red	Terrestrial	Recognition		●
	Ground-Based SAR	Terrestrial	Monitoring		●
Slides deep-seated	Aerial photogrammetry	Airborne	Recognition	●	●
			Monitoring		●
	HR/VHR	Satellite	Monitoring	●	●
	InSAR	Satellite	Recognition		
			Monitoring		
	Ground Based SAR	Terrestrial	Monitoring		
	Airborne Laser scanning	Airborne	Recognition		
	Terrestrial laser scanning	Terrestrial	Recognition		
			Monitoring		
Slides Shallow	Aerial photogrammetry	Airborne	Recognition	●	
	HR/VHR	Satellite	Recognition	●	●
	Airborne Laser scanning	Airborne	Recognition		
	Terrestrial laser scanning	Terrestrial	Recognition		●
	InSAR	Satellite	Recognition		
Flows	Aerial photogrammetry	Airborne	Monitoring		●
	InSAR	Satellite	Recognition		
	Airborne Laser scanning	Airborne	Recognition		●
			Monitoring		●
	Terrestrial laser scanning	Terrestrial	Recognition		
			Monitoring		

CHAPTER 3
Using InSAR for Landslide Recognition

3.1 Introduction to InSAR

The first satellite with Synthetic Aperture Radar (SAR) capabilities was launched on June 27th, 1978 (SEASAT) the same year as Navstar, the first GPS satellite. Experiments conducted by US jet propulsion laboratory showed that Interferometric InSAR was effective in monitoring changes but conducting additional research was difficult as more data was not readily available, and the computer technology was not advanced enough for easy processing of data. Around the same time the GPS technology gained traction and more advancements were made in its direction due to funding from the US Department of Defense (USDoD). In the 1990s pioneers like Massonnet (Massonnet & Adragna, 1990) showed multiple applications of SAR which brought new interest to the field, but the development was still slow as compared to other satellite technologies like GPS. This was due to the application of InSAR required a strong understanding of computer radar technology and geophysics, which was not usually the case as both topics were considered to be unrelated to each other. It is only in the last two decades that collaborations between radar specialists with geologists, civil engineers, and other related disciplines have brought this technology to the spotlight. In 2014 SENTINEL-1A was launched which is the first civilian sensor specifically designed for monitoring deformations over large areas. This can be considered the crown jewel in the development of InSAR (Ferretti, et al., 2007).

3.2 InSAR methodology

To understand how InSAR works, the basics of imaging with radar sensors and SAR are introduced first.

3.2.1 RADAR Sensor

The major difference between an optical imaging sensor and a radar imaging sensor is the wavelength at which they operate. The optical sensor operates at a wavelength of approximately 1(μm) and the Radar sensor in the range 4 cm- 10cm. A reference scale of the EM spectrum is shown in Figure 20 where it is evident that there exists a significant difference in wavelength. For the optical sensor, the light waves cannot penetrate the surface and the image obtained would be either clouds or the surface landscape. But in the case of radar sensor the longer wavelength implies that the waves can penetrate some media, including water, very dry soil, trees and clouds, among others. The ability to penetrate increases with an increase in wavelength. This property makes the radar imaging the preferred technique for some applications that cannot be done by optical imaging sensors (Richards, 2009).

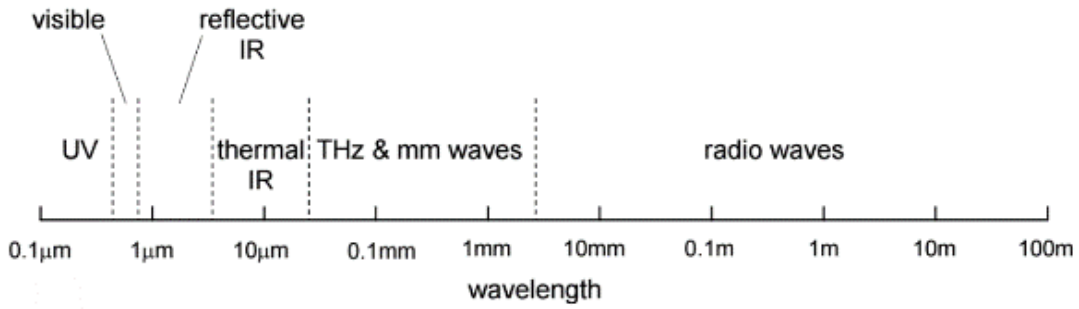

Figure 20: Reference scale for the EM

The energy source needed to view the target area is different for a Radar sensor. While the optical imaging uses the sun's visible and infrared light, the radar sensor transmits its own "light" to "illuminate" the target area as seen in Figure 21 where the energy emitted from the antenna illuminates the earth gets back to the platform. This is because the microwave energy transmitted by the sun and earth is too weak to be detected by the radar sensor to obtain meaningful data.

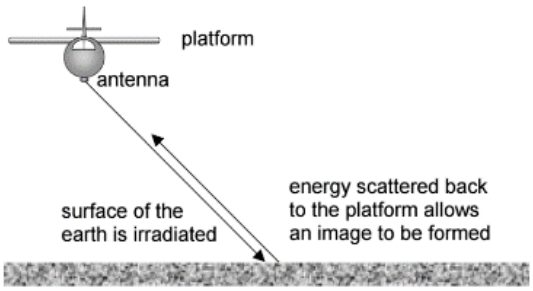

Figure 21: This image illustrates the working of an active radar sensor which illuminates its target with its own energy

3.2.2 Radar system

The active Radar system used for remote sensing consists of a transmitter and a receiver (Ferretti, 2014) and are classified as *monostatic*, i.e., both the transmitter and receiver share same antenna, and *bistatic*, i.e. transmitter and receiver are located separately on the platform. The monostatic remote sensors are widely used for remote sensing applications as compared to bistatic. The best approach to acquire an image with optical systems is to scan an area across the earth that is normal to system. However, this approach is not suitable for Radar systems as using this scanning approach would result in lower resolution and smaller wavelength, as the beam would be narrow. Instead, the radar system scans to its side as observed in Figure 22 which shows longer footprint as compared to scanning normal to the platform (Richards, 2009). The pulse emitted by the radar, travels to the target at approximately the speed of light, scatters and returns to the system at the same speed. The returned pulses are separated with respect to time to form the signal pattern of target terrain.

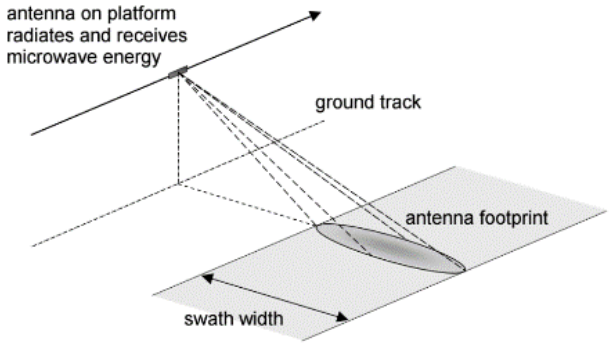

Figure 22: The radar imaging geometry

The pulse signal is commonly called ranging pulse and the rate at which they are repeated is called Pulse Repetition Frequency (PRF). The PRF is synchronized with the platform so that the strips of land are covered continuously, pulse by pulse. This is visualized in Figure 23 where large strips of terrain are covered with every successive pulse.

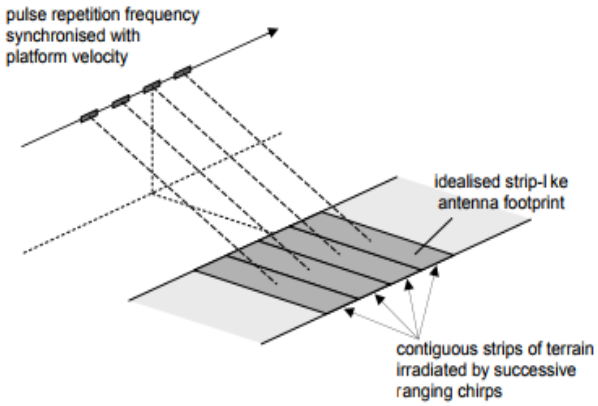

Figure 23: Successive ranging pulses are transmitted synchronously with platform velocity to cover most of the terrain

One of the major restrains for PRF is that if all echoes from a transmission are not returned before the next transmission range then ambiguity occurs, the data is corrupted and distance of target is no longer accurate. This is prevented by restraining PRF with respect to slant range and velocity of the satellite. Therefore, the highest possible PRF is bound to the largest slant range (direct line from radar to a point on the ground) of the system. The maximum usable PRF is further discussed in (Richards, 2009)

3.2.3 Radar Signal

Most Radar systems in remote sensing use monochromatic signals (Ferretti, 2014). A monochromatic signal is a sinusoidal signal at the central frequency. This is evidenced as a sinusoidal arrangement of the EM field, i.e., when the signal is “frozen” in time the

EM field will have constant sinusoidal pattern throughout. If the same experiment is conducted to a light bulb, i.e. observing the frozen EM field, we would see that none of the fields will have any fixed relationship to the other within the beam. Since the radar sensor is coherent, the beam follows a constant pattern. To achieve this constant transmitted signal the signal is modulated to a carrier frequency, so the transmitted signal remains identical. This is also called modulation.

The returned signal (echo) is demodulated, i.e. the echo which is an analog signal is multiplied by the original carrier function and with a 90-degree shifted version of the signal (Figure 24). Through demodulation and after filtering the real and imaginary part of the complex number of the respective pixel is obtained. This process is done by the satellite and the concept is explained in detail in (Ferretti, 2014)

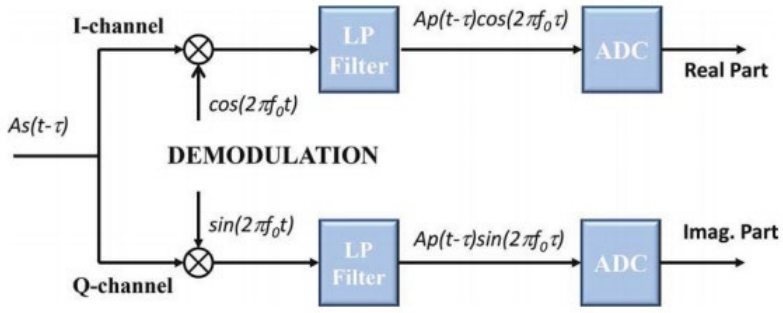

Figure 24: Simplified diagram of the radar receiver showing the creation of real and imaginary part of the image from which the phase and amplitude are developed

3.2.4 Radar Image

The radar image is formed as follows. The moving satellite fires a burst of microwave signals at an angle from its side. When this signal reaches the surface of the target, part of the signal is lost, and the rest is scattered. Since the signal is fired from a moving platform (e.g. satellite) at a slant angle the backscatter returns in delayed time with respect to the orthogonal direction of the satellite. This helps in locating the position of the target in the orthogonal direction. Since the platform will be firing the signal in bursts the intensity of the signal with respect to a target location will increase and decrease with successive bursts until the target leaves the footprint of the signal, this helps in determining the location of the target with respect to the satellite path. From the above we can find the signal with respect to each target location. The signal is converted from analog to digital by demodulating with respect to two channels which produce the real and imaginary part of the complex number. These details are then used to create the amplitude and phase of a radar image.

The radar imaging systems are divided into Real Aperture and Synthetic Aperture. Real aperture fires small bursts while synthetic aperture can cover large areas. For covering a large area as such needed in landslide analysis synthetic aperture is most suitable.

3.3 SAR

To understand how SAR is advantageous the resolution in Real Aperture is introduced first. The Real Aperture resolution in azimuth direction can be measured as (Thomas M. Lillesand, Ralph W. Kiefer 1989):

$$r_a = \frac{\lambda}{l_a} R_a \quad (1)$$

where

r_a = Resolution in azimuth direction

λ = Wavelength of signal

l_a = Antenna length in azimuth direction

R_a = Slant range distance or Distance to target

The above equation suggests that for a satellite flying at 1000km altitude with 3m long antenna and 3cm wavelength will have a Real Aperture resolution of 10km. For obtaining a resolution of 1m the satellite will need to either fly close to earth or increase the length of its antenna to impractical scales. To counter this, Carl (Carl, 1951) suggested the concept of synthetic aperture. He proposed that one can simulate a large antenna by predicting the reflected signal location, when the signal is launched at an angle. Using this concept, the length of the antenna becomes the footprint of the antenna. This would mean that the size of the antenna can increase to a massive scale and resolution in range of meter is achieved. Then equation (1) for azimuth resolution becomes:

$$r_a = \frac{l_a}{2} \quad (2)$$

The above equation implies that synthetic aperture is more practical since good resolution images can be obtained with relative short antennas. The details of the derivation of equation (2) are reported in (Richards, 2009).

3.4 InSAR

The previous sections discussed how radar imaging can cover large area with synthetic aperture. The sensor is also able to detect deformation in order of millimeter by combining, or interfering, signals from two antennas that are separated spatially or temporally. The radar signals from the two acquisitions will travel distance of r_1 and r_2 to antennas A_1 and A_2 respectively. The difference between r_1 and r_2 will result in the signal being out of phase by some phase difference ranging from 0 to 2π if the geometry of the interferometric baseline, i.e., the distance between the two antennas, is known. This distance is known to a high degree of accuracy which helps to obtain the phase difference that is used to calculate the elevation of a point.

There are multiple ways of collecting Interferometric radar data. The basic approach is the *single-pass interferometry* in which a satellite carries two antennas, one antenna acts as both the transmitter and receiver, but the second antenna acts only as a receiver. The interferometric baseline is the distance between the antennae which result in a low error

when detecting the elevation of a target. The other type is the *repeat-pass interferometry* in which a satellite carries only one antenna which acts as both transmitter and receiver. To obtain the elevation of the target the satellite needs to travel two times over the target and to minimize the error the second pass must have a baseline less than 10 meters. From this definition, it seems that repeat-pass interferometry has high complications, but when the purpose of the satellite is to monitor a region like in the case of landslide investigation then this process becomes advantageous. Applications where InSAR is advantageous include measuring the glacier movement, the detection of moisture content in soil by obtaining the surface moisture and subsidence of a city due to the pumping of water, among others.

A SAR image contains information on the amplitude and phase of the reflected signal. The deformations estimation is based on the phase value. Mathematically, the phase value, $\Phi(\mathrm{P})$, of single acquisition of a pixel, P, having its coordinates in range and azimuth can be written as (Ferretti, 2014)

$$\Phi(P) = \varphi + \frac{4\pi}{\lambda} r + \alpha + \nu \tag{3}$$

where:

φ is the reflectivity phase. This factor takes into consideration that total reflection does not take place and scattering occurs due to target/location;

$\frac{4\pi}{\lambda}$ is the location of "electromagnetic barycenter "of all elementary scatterers, λ being the wavelength of the signal;

r is the sensor to target distance;

α is the effect of the atmosphere on the electromagnetic wave. The quality of the final result depends on this factor; and

ν depends on noise or more importantly the thermal noise of the radar system.

The phase value of a single SAR image has no use because the contribution of the different phases cannot be separated, and all the wrapped phase values seem to be unrelated. This is where the concept of SAR Interferometry comes in by introducing the difference in the phase values of each pixel "P" from two acquisitions. Equation ($\Phi(\mathrm{P}) = \varphi + \frac{4\pi}{\lambda}\mathrm{r} + \alpha + \nu$ (3) becomes

$$\Delta\Phi(P) = \Delta\varphi + \frac{4\pi}{\lambda}\Delta r + \Delta\alpha + \Delta\nu \tag{4}$$

An interferogram is developed by calculating the phase difference of individual pixels. In case of *single pass interferometry* all the parameters in equation (4) other than Δr vanish and Equation (5) becomes

$$\Delta\Phi(P) = \frac{4\pi}{\lambda}\Delta r \quad (5)$$

Different procedures are performed to mitigate the effect of errors in the phase of an image. These include choosing existing DEMs to predict the phase value and reducing the perpendicular baseline.

3.5 DInSAR

Differential SAR Interferometry is an interferometric technique to analyze and quantify the surface movement. This is done by removing the effect of topography in the area of interest. This process can be better understood by progressing from the phase equation (5). By removing the topographic phase, the phase of surface deformation is clearly visible

$$\Delta\Phi_D = \Delta\Phi(P) - \Phi_{topo} = \Phi_{displacement} \quad (6)$$

Where

$\Delta\Phi_D$ Is the Differential phase

Φ_{topo} Is the simulated topographic component (The topographic component is simulated from existing topographic data)

The above equation is used to remove the effect of topographic related phase components. The removal of the topographic phase is necessary to estimate the change in landmass or displacement of landmass. This is done by using an existing Digital Elevation Map (DEM) of the area of interest from previous acquisitions and generating a synthetic interferogram, which is then subtracted from the interferogram generated by equation (5). This means that the accuracy of the DInSAR depends on the existing DEM, however the DEM error can be estimated and compensated as mentioned in (Ferretti, et al., 2007). However, due to the high accuracy of the GPS receivers onboard satellites, DEM errors are negligible. They generally exist in areas where the topography changes frequently and it is tough to get new and accurate DEM's.

3.6 PSInSAR

PSInSAR is an advanced InSAR technique that is capable of measuring displacements in the order of a millimeter. PSInSAR stands for Persistent Scatterer Interferometric Synthetic Aperture Radar and is a reliable time series analysis for ground deformations using SAR images. It was first developed by Ferretti and his colleagues (Ferretti, et al., 2000) to address decorrelation of the interferograms that were giving unreliable deformation maps. The process involves isolating stable pixels with high coherence conveniently called Persistent Scatterers (PS) and observing their displacements. In the field these PS can be any objects like rocks, roofs, etc. The only requirement for a PS is that it shows high coherence over the entire time series. The PSInSAR analysis is highly accurate as compared to traditional DInSAR analysis as pixel readings that are unreliable are discarded. Various PSInSAR algorithms are reviewed in (Crosetto, et al., 2016) but the core concept of isolating the coherent signals has not changed.

3.7 SAR Satellite Wavelength

Radar satellites are divided based on the wavelength of their signal (UNAVCO, 2015). The X-Band has the shortest wavelength and is approximately 3cm and is used by the military for maritime monitoring. The L-Band has the highest wavelength and is used for monitoring activity in high vegetation. Figure 25 summarizes different satellite missions, their duration and their wavelength. For the analysis in this work, Sentinel-1 satellite data is used Sentinel-1 is a C-band satellite implying a wavelength between 4cm – 8cm. C-band wavelength is used for monitoring in cities. Different wavelengths behave in a unique manner when they react with the surface. In general, the shorter the wavelength the better it is to detect ground motion. However, a shorter wavelength has its disadvantages in obtaining coherent images (Agram, 2013).

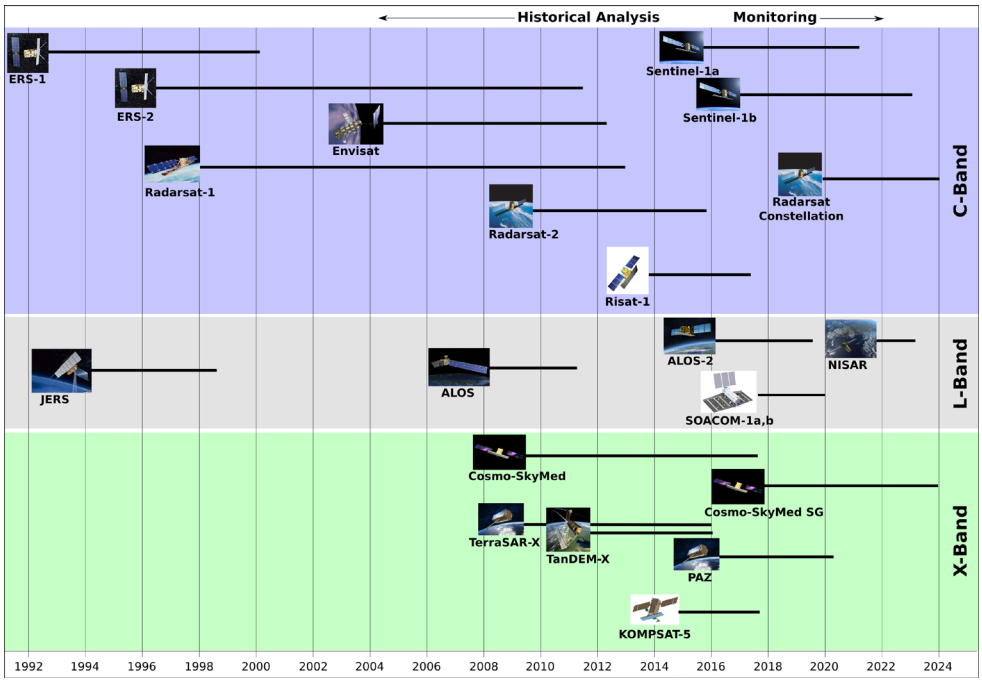

Figure 25: Present and past SAR satellites (UNAVCO, 2015)

Radar penetration is graphically depicted in Figure 26 and outlined next, in view of the effects of vegetation, dry soil conditions, and ice.

3.7.1 Vegetation

In general, L-band signals can penetrate leaves and trees, C-band signals can penetrate through minor vegetation, while X-band signals are reflected by leaves. Therefore, L band sensor is ideal to measure displacements in areas with high vegetation landscape while C and X bands are useful for measuring displacement in an urban landscape.

3.7.2 Dry soil conditions

For dry soil conditions, the L-band signal penetrates dry soil and is ideal for measuring soil moisture content, while the C-band partially penetrates dry soil and X-band is reflected by the surface roughness.

3.7.3 Ice

When ice covers the surface of the target, the L band signal can penetrate the ice layer completely. The C-band signal partially penetrates the ice; however, the X-band cannot penetrate the ice layer and is ideal for measuring glacier displacements

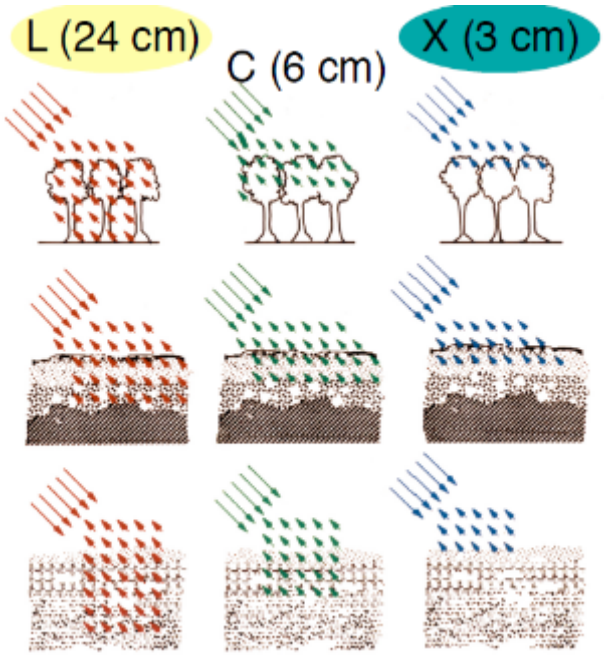

Figure 26: Microwave penetration of different SAR sensors (Fielding, 2016)

CHAPTER 4

DInSAR Implementation

In view of the satellite image processing methodologies studied in this feasibility study it was concluded that the DInSAR methodology is the most promising for detecting ground movement over a period of time. This chapter discusses the software and the implementation procedure of the DInSAR technique to detect landslides.

4.1 Software

Two open sourced programs are used in this feasibility study, i.e., SNAP and SNAPHU.

SNAP is a part of Scientific Toolbox Exploitation Platform (STEP) and stands for Sentinel Application Platform, which is jointly developed by the European Space Agency (ESA) with help from Brockmann Consult (Brockmann Consult, 2017) and Array systems computing (Array Systems, 2017). Since the program is open source the community is active in *forum.step.esa.int* where all the questions related to the program are discussed. Some of the developers who moderate the forum also consider the suggestions that appear in the forum to improve the program. Unlike other SAR programs SNAP shifted from code based to interface based to make the program more accessible.

SNAPHU is used to perform 2-D phase unwrapping and is an implementation of the Statistical-cost, Network-flow Algorithm for Phase Unwrapping proposed by Chen and Zebker. The open source code can be downloaded from ESA's site (ESA, 2018). For phase unwrapping SNAPHU is the most reliable tool as it can perform a lot of computationally expensive problems (Chen & Zebker, 2002).

The data obtained from Sentinel-1 is processed using SNAP following the steps mentioned in Figure 27 and discussed following. The steps mentioned below are repeated for each data set and the results are studied separately (Veci, 2016). The Etna showcase study discussed in detail in Chapter 5 is used to demonstrate the results of each implementation step. Mount Etna is an active volcano in Sicily, Italy, covering an area of 459 square miles. The most recent eruption during the course of this study was on the 16th of March 2017. Sentinel 1 data used to analyze the effect of Etna eruption is acquired on February 2, 2017, March 3, 2017, March 14, 2017, and March 26, 2017.

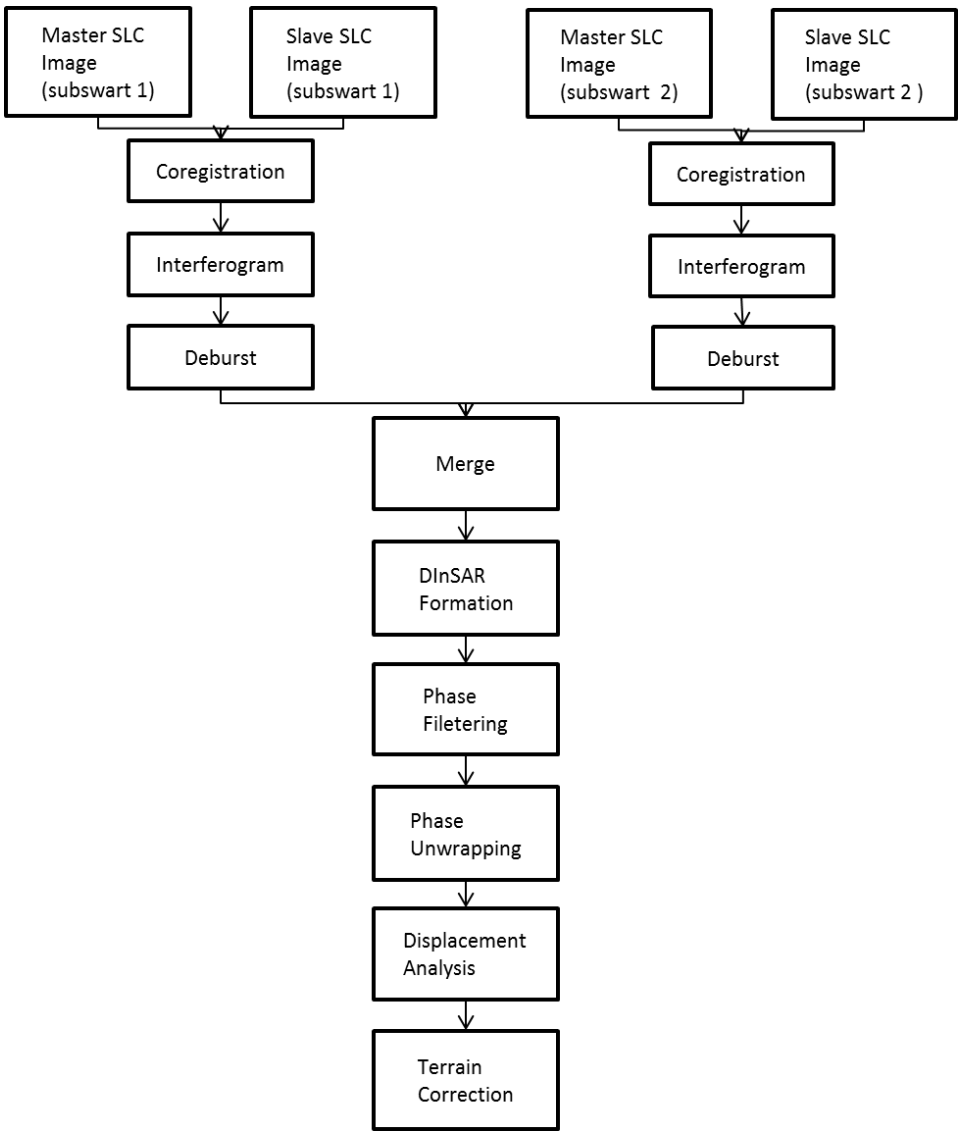

Figure 27: Flowchart followed for DInSAR analysis

4.2 Step-1 Coregistration

Coregistration is the critical step in which pixel to pixel matching is performed on two acquisitions so that accurate phase difference can be calculated in order to increase coherence and reduce the noise. To coregister the two images one image is chosen as the master and other is the slave. The slave image is superimposed on the master, and, typically the older image is chosen as the master as this helps in the detection of deformation in later stages. Orbit files are applied to each acquisition and resampling is done to complete the coregistration process. The orbit files provide accurate position and velocity of the satellite for the time of acquisition. For this study TOPSAR data is used which is split into 3 parts called sub swaths and the sub swath with the target image is processed. This is done to prevent the processing from becoming computationally expensive. During the splitting process, the polarization of the images is also chosen. The

polarization of master and slave must be the same to prevent errors. The above steps can be performed in SNAP individually or in a single step using the S-1 TOPS coregistration option. Figure 28 shows the intensity of the datasets recorded on March 14 and 26th 2017. Demarcation zones are evident as the black horizontal lines.

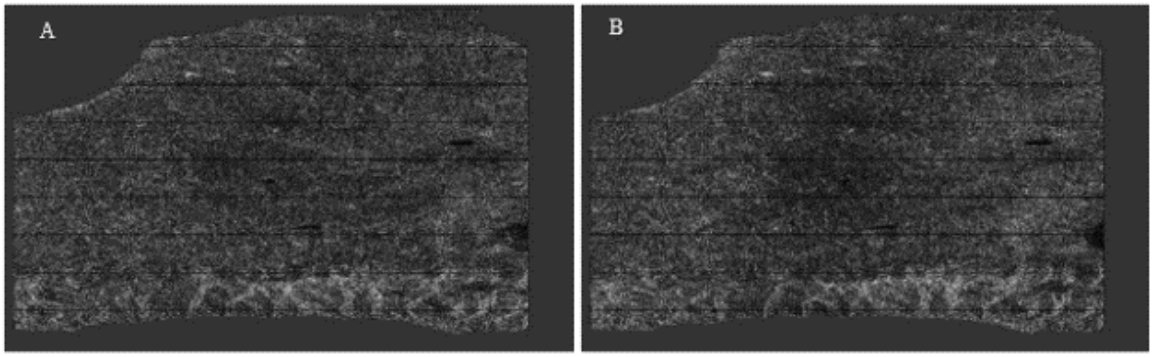

Figure 28: Intensity part of datasets taken on (A) March 14 and (B) March 26th 2017 used in the image coregistration

4.3 Step-2 Interferometric process.

In the coregistration step the pixel values are aligned. To develop an interferogram, the phase value of the slave is removed from the master as per equation (3). However, equation (3) does not generate accurate interferogram as it does not consider the flat earth phase. Due to numerous reasons such as the earth being an irregular ellipsoid, and the satellite tilt, additional phase element is present during the generation of the interferogram, introducing, thus, an error in the interferometric phase. This error is called the flat-earth phase. The flat earth phase can be computed from the perpendicular baseline and removed to generate a better interferogram. In SNAP the flat earth phase is removed during the interferogram formation. Figure 29 shows the interferogram corresponding to coregistered images in Figure 28 before any filtering is applied.

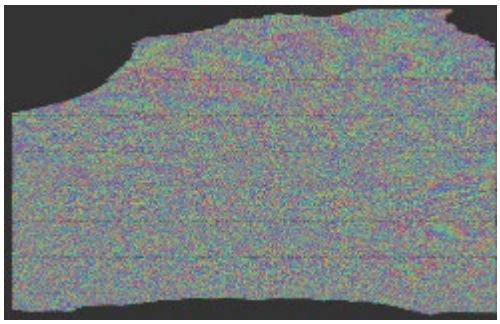

Figure 29: Interferogram corresponding to coregistered images of Figure 28 before any filtering is applied; demarcation zones are still visible

4.4 Step-3 Deburst

This step is performed exclusively to acquisitions taken through TOPS technique. This is because in TOPS the satellite covers long strips of an area that are separated by demarcation zones. These demarcation zones contain random values and need to be

removed through debursting so that these zones will not affect future processing. Deburst is done in SNAP using the TOPS-DEBURST option. Figure 30 demonstrates the result of the debursting step on the Etna images.

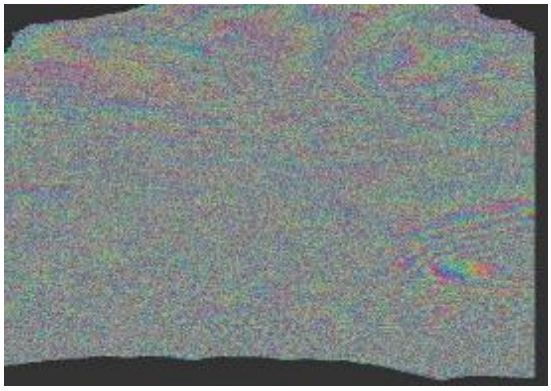

Figure 30: Interferogram with demarcation zones removed after debursting

4.5 Step-4 Merge

This step is also performed almost exclusively to acquisitions taken through the TOPS technique. This step is performed if the target area is located in more than one sub swath. All the above-mentioned steps are repeated to each sub swath and they are merged using the TOPS merge option in SNAP. In the Etna case study, the volcano is located between subset 1 and subset 2. Figure 31 shows the interferogram after merging of the subsets.

Figure 31: Interferogram in Figure 30 after merging of the two subsets

4.6 Step-5 Topographic phase removal

Topographic phase removal is used to generate the DInSAR phase. The topographic phase is estimated from existing DEM. If the target area is not located near the poles the existing DEM used is SRTM. By removing the topographic phase, the resulting phase will have the ground motion phase visible, although additional filtering needs to be done for better image resolution. In SNAP multiple DEM options are available to perform this step and they must be considered based on the location and satellite used for acquisition. Some locations are not covered by existing DEMs this is because of the satellite paths

and the targets geo coordinates need to be compared before choosing the right DEM. Figure 32 shows the result of the Etna case study after the topographic phase removal step, Although the displacement phase is now visible, significant noise is still present.

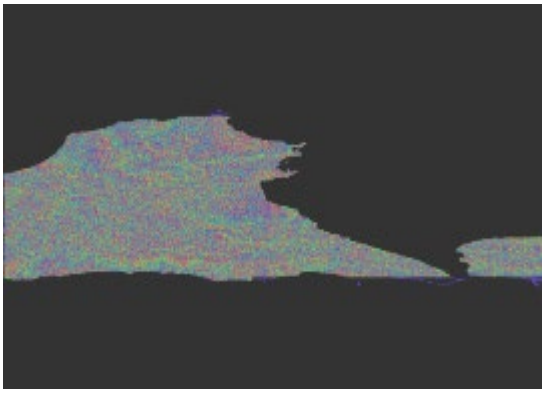

Figure 32: The topographic phase has been removed in the Etna case study

4.7 Step-6 Phase filtering

This step is optional but is recommended as this step reduces the noise, helps in product visualization and increases the accuracy of the phase unwrapping process. For phase filtering the algorithm developed by R.M Goldstein and C.L Werner (Goldstein, 1998) is used as this method produces the best results for Geophysical applications. In SNAP a separate option is available to perform Goldstein phase filtering.

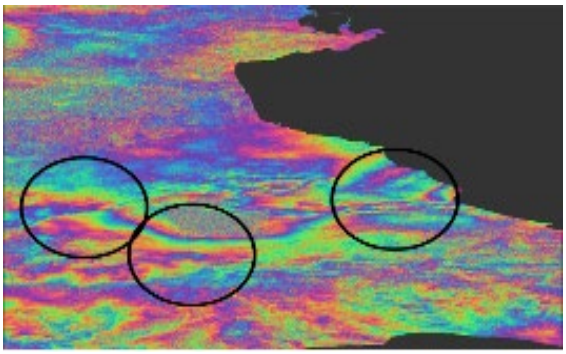

Figure 33: Displacement phase after filtering is clearly visible in the highlighted areas

4.8 Step-7 Phase unwrapping

From Step-6 the ground motion can be observed but actual displacement cannot be measured. To develop the displacement maps the wrapped phase should be converted to continuous form. This process is performed in SNAPHU. The result from Step-6 is exported to SNAPHU where after the unwrapping is completed the finished product is imported back to SNAP to perform the final part of the test. This step cannot be represented graphically.

4.9 Step-8 Displacement analysis

The unwrapped phase is imported back to SNAP and converted to displacement. The displacement generated is the displacement in the direction of the line of sight of the

satellite. In SNAP the unwrapped phase can directly be converted using the phase to displacement option. The result of this operation is shown in Figure 34.

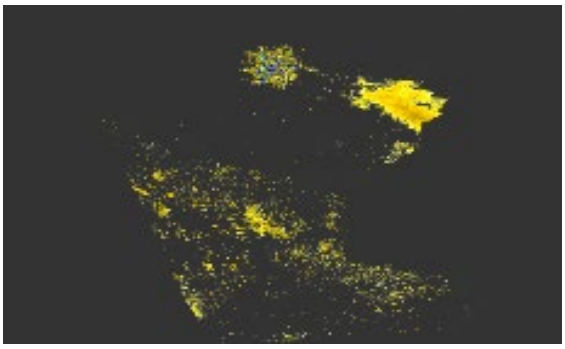

Figure 34: Displacement in the direction of satellite line of sight

4.10 Step-9 Terrain Correction

Terrain Correction is a necessary step to remove the misleading influence of topography on backscatter values and satellite tilt. These distortions are removed by using the metadata available with the reading or by using external precise orbit with reference DEM data to derive precise geolocation information. This correction can be performed after any step, but after terrain correction no additional processing can be done. This step is performed on data that needs to be exported to google earth for observations, as demonstrated in Figure 35.

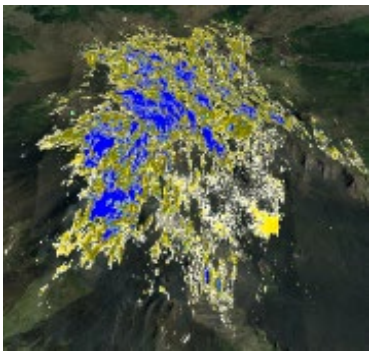

Figure 35: Displacement map superimposed on Google Earth file

CHAPTER 5

PSInSAR Implementation

5.1 Software

Two open sourced programs are used in this feasibility study, i.e., SNAP and StaMPS.

SNAP is jointly developed by the European Space Agency (ESA) with help from Brockmann Consult (Brockmann Consult, 2017) and Array systems computing (Array Systems, 2017) and has been discussed in Section 4.1. StaMPS is a software package that implements the Stanford Method, an InSAR sersistent scatterer method. The method was originally developed at Stanford University and further expanded at the University of Iceland and Delft University of Technology. StaMPS is chosen in this work for its ability to detect ground motion also in rural areas where man-made structures that could be identified as the persistent scatterers are sparse or do not exist. Details on the theoretical background are reported in (Hooper & Zebker, 2007) (Hooper, 2008) (Hooper, et al., 2004)

5.2 Methodology

The analysis is conducted in two stages. The first stage involves the interferogram formation and is performed using toolbox SNAP. The second stage involves the PS analysis and is performed using StaMPS.

The algorithms for both stages are shown in block diagram (1&2) respectively.

5.2.1 Interferometric stack formation.

In this stage a master image is identified (ref) and the rest of the images (slave) are co-registered to it. Co-registration is done to align all the pixels of the slave images to the master. After co-registration, debursting (Section 4.4) removes demarcation zones present in the images. Since the stack of images covers a large area, the SLC data can be cropped to include only the study area to make the process computationally feasible. From the cropped stack interferograms are developed and additionally the topographic phase is also removed in this step (Section 4.6). The process of removing topographic phase from an interferogram is called Differential Interferometric SAR (DInSAR) and is performed to obtain the ground motion (Section 4.9). The stack is then geocoded to estimate the position of every pixel using orbital parameters (Section 4.10). The block diagram in Figure 36 demonstrates the sequence of activities for forming the interferometric stack.

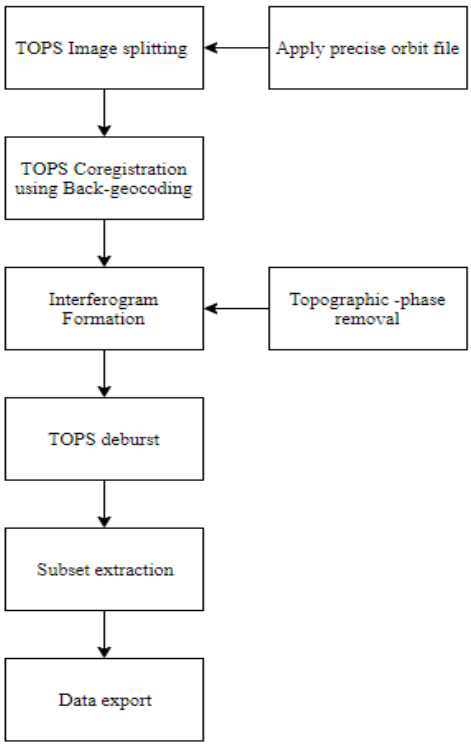

Figure 36 Block diagram showing the basic steps for forming the interferometric stack

5.2.2 PSI process

The stack obtained in the above stage is used in the Persistent Scatterer Identification (PSI) process to extract ground subsidence. The PSI is performed using StaMPS in MATLAB. Most of the PS identifying techniques assume a temporally linear deformation model. This restricts the use of such methods when observing fast moving landslides, the sudden change observed due to the landslide would make the associated PS invalid. This restriction and the underlining assumption is not present in the StaMPS algorithm. StaMPS, on the other hand, uses spatial correlation of the phase without any prior temporal assumptions. This also helps in the identification of PS in a non-urban setting which is ideal for this analysis. The process begins with identifying the PS based on their amplitude dispersion. Then the PS are filtered using the phase noise estimation and other filtering methods. The identified PS are unwrapped, and the subsequent displacement of each point is obtained. The results are in mm/year and can be better visualized in Google Earth. The block diagram shown shows the sequence of steps in PSI stage.

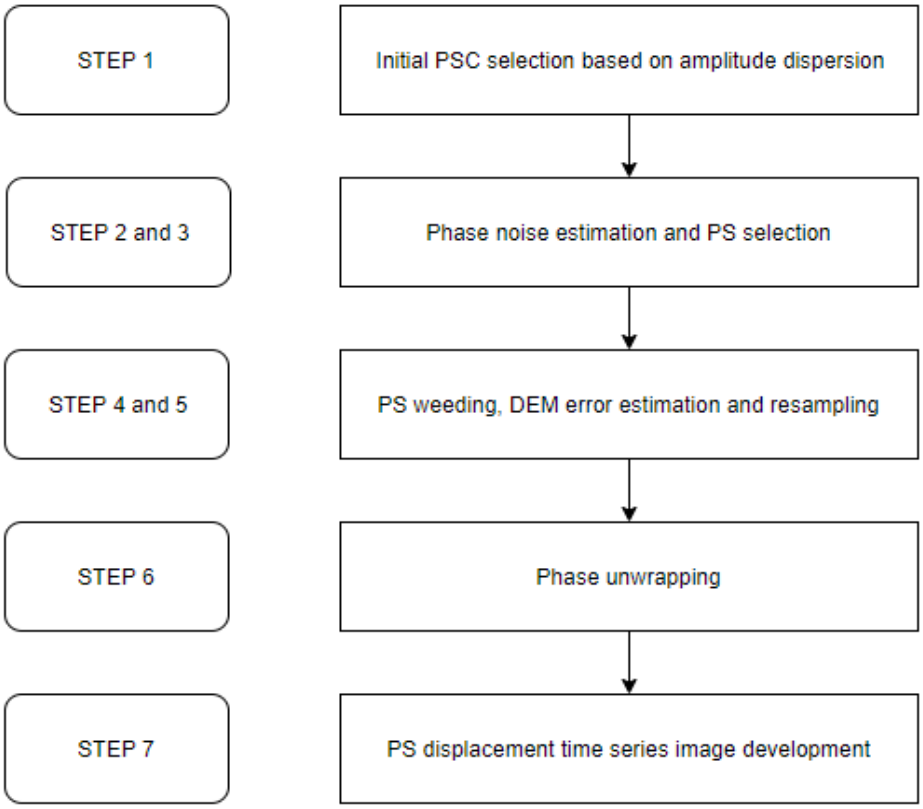

Figure 37 Block diagram showing the dequence of steps fof PSI analysis

5.3 Analysis

In PSInSAR analysis we are observing the displacement of persistent scatterer near the points of interest, e.g. railway tracks. Observing the displacement provides insight whether the area around the tracks is stable and if any unstable elements can cause disruption to the tracks. The unstable elements can be characterized by the slow subsidence buildup and generally fail when acted upon by triggering events like rainfall, earthquake, etc. The failure event may or may not occur, but this analysis can be used to detect high probability locations most likely to experience such events.

CHAPTER 6

DInSAR Showcase Studies

Two areas have been selected to demonstrate the implementation of the DInSAR methodology, i.e., Mount Etna in Italy, and Highway 1 in California USA. In both areas massive landslides have occurred in the last two years due to different triggering mechanisms.

6.1 Satellite information

For landslide analysis data from Sentinel-1mission is used. Sentinel-1 is a polar-orbiting radar mission which has 2 satellites Sentinel-1A and Sentinel-1B. They were both launched respectively on 3 April 2014 and 25 April 2016 using Soyuz rocket from the European spaceport in French Guiana. Each Sentinel-1 satellite passes a target area every 12 days and would cover the entire world mass. The satellite is expected to transmit data for 7 years at minimum and have fuel for 12 years (ESA, 2016).

Sentinel-1 mission uses C-band imaging radar with 4 imaging modes and coverage up to 400km. It provides dual polarization capabilities with short revisit times (12 days). The datasets are named following the convention shown in Figure 38. For DInSAR, Single Look Complex(SLC) data type is used (ESA, 2017)

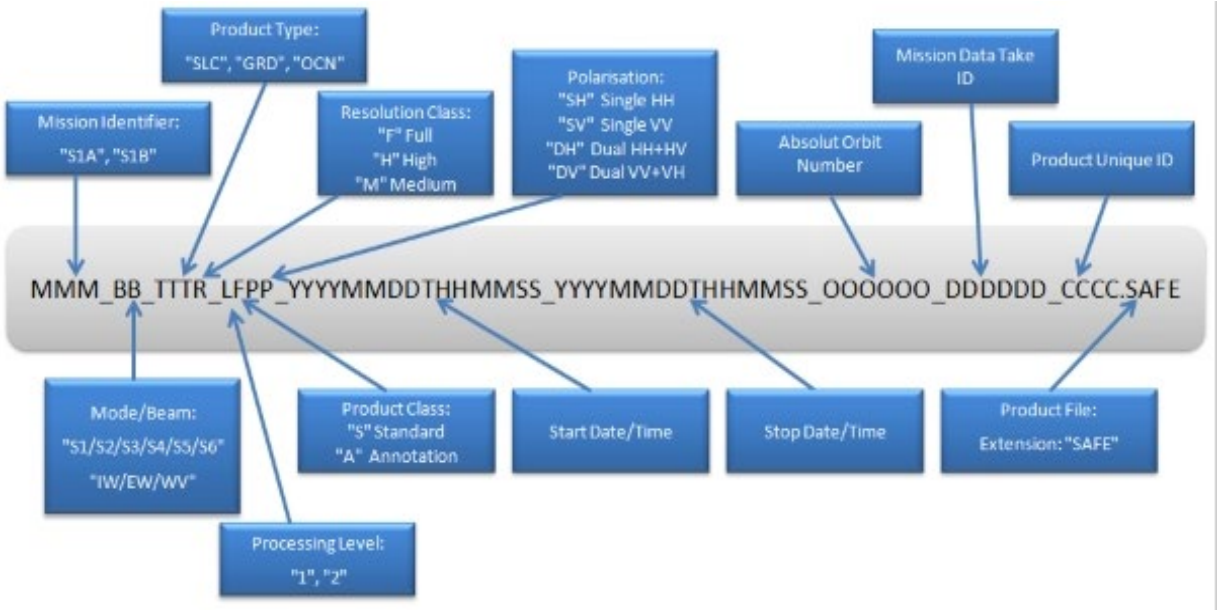

Figure 38: Dataset naming convention

For DInSAR analysis SLC type acquisitions are used. Single Look Complex (SLC) images have focused SAR data and the pixels are spaced equally in azimuth direction and in slant range. The data is represented as complex numbers containing both phase and amplitude. SLC products are used for applications where the full bandwidth and phase information are required (AIRBUS defence and space, 2014).

6.2 Study Area: MOUNT ETNA

6.2.1 Mount Etna Area Description

Mount Etna is an active volcano covering an area of 459mi^2 which had the most recent eruption during this study on 16 March 2017. The volcano is located in Sicily, Italy. Sentinel 1 data used to analyze the effect of Etna eruption is acquired on February 2, 2017, March 3, 2017, March 14, 2017, and March 26, 2017. The corresponding satellite image files (datasets) are:

1. S1A_IW_SLC_1SDV_20170218T165557_20170218T165624_015341_01927E_40B5.SAFE
2. S1A_IW_SLC_1SDV_20170302T165557_20170302T165624_015516_0197CF_B591.SAFE
3. S1A_IW_SLC_1SDV_20170314T165558_20170314T165625_015691_019D20_0A0A.SAFE
4. S1A_IW_SLC_1SDV_20170326T165558_20170326T165625_015866_01A24E_E6CA.SAFE

The aim of this analysis is to see the effect of the volcano on the topography and to detect any possible landslides that are developed because of it.

6.2.2 DInSAR Analysis

DInSAR analysis is performed using SRTM DEM as reference to develop phase maps of the area. Total of 3 interferogram phase, coherence and subsequent displacement maps are shown to analyze the effect of volcano to generate landslides in the region. The coherence is high in all 3 cases due to the fact that this is a volcanic region with minimum vegetation. Figure 39 shows Mount Etna taken on June 5,2014 by Landsat mission. All images have been terrain corrected and exported to google earth for easier understanding

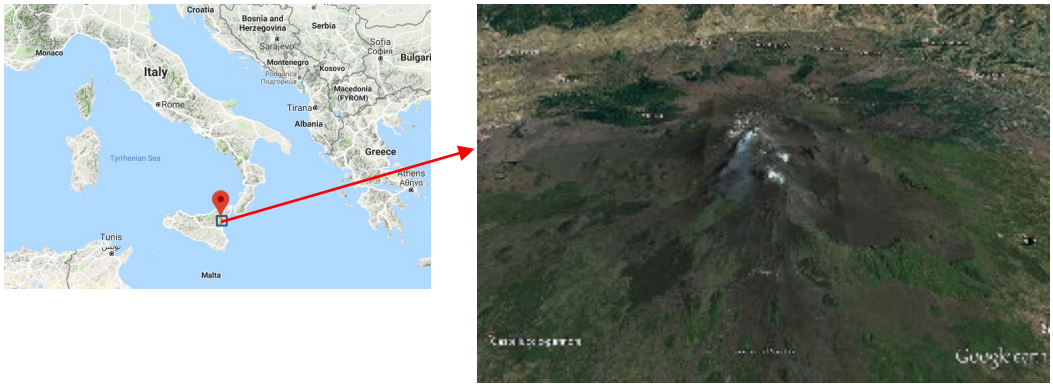

Figure 39: Mount Etna, Italy, observed through the visual spectrum. This image shows the target area to be analyzed

6.2.3 Test 1

For this test, acquisitions taken on February 18,2017 and March 02, 2017 are analyzed. Figure 40(a) shows the phase reading of the region. From the image, we can see that there is no slope instability. The minor phase contours around the decolor zone suggest minor uplift in the crust. Figure 40(b) shows the coherence map of the region. From the coherence map we can see that other than around the crater, the image has consistent

high signal to noise ratio indicating higher reliability of the phase data. The crater has low coherence due shadowing. Figure 40(c) shows the displacement analysis map of the region. The region with high subsidence (blue) cannot be considered as this region is under the poor coherence.

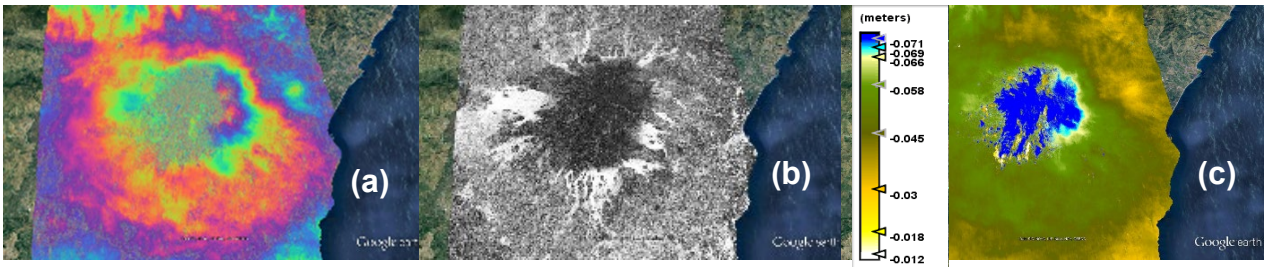

Figure 40: Test 1: (a) Phase map shows no significant variations that signify slope instability; (b) Coherence map shows low signal strength near the crater; (c) Displacement map showing a minor subsistence around the crater

6.2.4 Test 2

For this test, the acquisitions taken on March 02,2017 and March 14,2017 are analyzed. Figure 41(a) shows the phase of the region and no major slope instability can be seen in the image. Figure 41 shows the coherence map of the region and from the map we can see that the crater of mount Etna shows poor coherence, as in test 1. Figure 41(b) shows the coherence map of the region and from the map we can see that the center of the mount has poor coherence(black). Figure 41(c) shows the displacement analysis map of the region. No significant variation of the displacements is observed; however, the constant subsidence is probably attributed to calibration inaccuracies.

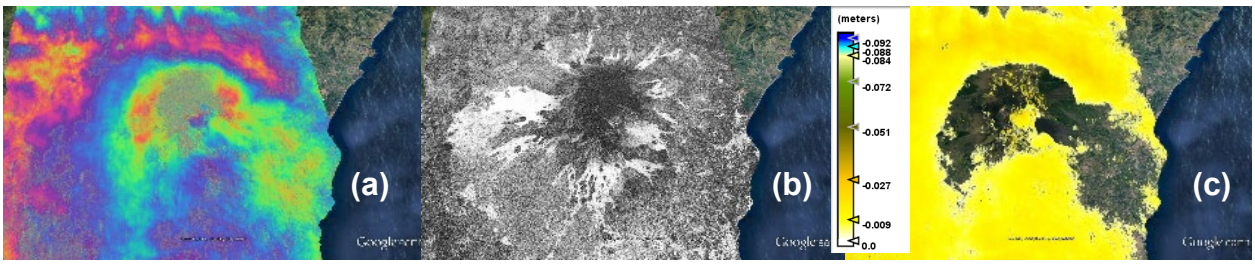

Figure 41: Test 2: (a) Phase map shows no significant variations that signify slope instability; (b) Coherence map shows low signal strength near the crater; (c) Displacement map showing a minor subsistence around the crater

6.2.5 Test 3

For this test, acquisitions taken on March 14,2017 and March 26,2017 are analyzed. It is noted that the eruption took place on March 16 of the same year and this test captures the before and after configuration. Figure 42(a) shows the phase of the region where significant phase activity is present. The color changing contours signify the slope instability and possible landslide activity in the region. Figure 42(b) shows the coherence map of the region. It is seen that the volcano's crater has poor coherence (black) and

measurements inside the crater are not reliable. Figure 42(c) shows the displacement analysis map of the region. The displacement map covers the volcanic event. Other than the zone with poor coherence the displacement activity is in the order of 10 cm.

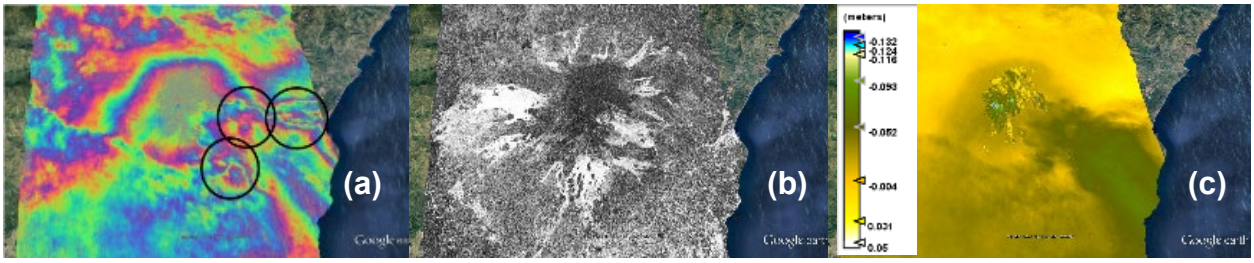

Figure 42: Test 3: (a) Phase map shows slope instability and possible landslide activity; (b) Coherence map shows low signal strength inside the crater as in the other tests; (c) Displacement map showing a displacement activity in the order of 10 cm

6.2.6 Discussion

Considering the 3 analyses we can observe that the images have high coherence. High coherence images generate accurate interferograms from which ground motion can be easily detected. In Figure 40(a), Figure 41(a) and Figure 42(a) we can see that the center of the Etna crate has high noise and this is due to the principle of shadowing and layover. In these cases the signal cannot return back to the satellite, because it is prevented from returning by the crater walls. The phase from test-1 and test 2 show that there is low seismic activity in the region. Test 3 which covers the eruption shows multiple fringes (highlighted regions) which represents the slope instability and possible landslide activity. The coherence map represents the signal to noise ratio, with white being 1 i.e. full signal strength and black being 0 i.e. meaning no backscattering signal. The coherence in all three tests is consistent with the slope of the mount having high coherence and the volcanic crater having low to nonexistent coherence. This is also due to the direction of the satellite flight path and can change if the satellite path is different. The path of satellite in all 3 cases is ascending that means the satellite is travelling from south to north.

The displacement maps show the displacement in the direction of satellite line of sight. The negative sign represents subsidence. The displacement observed in each test is the displacement taking place between the two acquisitions. Finally, the accuracy of the displacement maps is not definitive and must be correlated with in-situ readings to calibrate the displacement data and estimate the error due to vegetation. It should also be noted that the phase change associated with landslide activity that have been highlighted in Figure 42(a) are not visible in displacement map in Figure 42(a). Additional phase elements might also affect the displacement maps that have not been properly removed in the analysis stage and further investigations should be contacted which are beyond the scope of this feasibility study.

6.3 Study Area: California Highway 1

California State Route 1 is a major highway along the pacific coastline shown in Figure 43(a). The route is 655.8miles and is the longest state route. A major mudslide occurred on May 20th, 2017 causing major disruption to traffic. An aerial image of the landslide is

shown in Figure 43(b). The global coordinates of the landslides are covered by Latitude 35.8709 Longitude -121.4382 and Latitude 35.8592 Longitude -121.4225. For the analyses in this work, we will use Sentinel 1 data of the area, acquired on April 25, 2017, May 07, 2017, May 19, 2017, and May 31, 2017. The aim of this analysis is to see if the landslide can be predicted by using DInSAR technique. The corresponding satellite image files (datasets) are:

1. S1B_IW_SLC_1SDV_20170425T020606_20170425T020633_005311_0094E3_4593.SAFE
2. S1B_IW_SLC_1SDV_20170507T020607_20170507T020634_005486_0099D1_B25E.SAFE
3. S1B_IW_SLC_1SDV_20170519T020608_20170519T020635_005661_009EA1_7930.SAFE
4. S1B_IW_SLC_1SDV_20170531T020608_20170531T020635_005836_00A3AE_1AA5.SAFE

DInSAR analysis is performed using SRTM DEM as reference to develop phase maps of the area. Total of 3 interferogram phase, coherence maps are shown to detect changes that would signal landslide activity. The displacement map of the area is not developed due to the process being computationally expensive to develop within the limited resources of this feasibility study. Figure 43(c) and (d) show the Landsat satellite imagery of the highway before and after the landslide event, respectively.

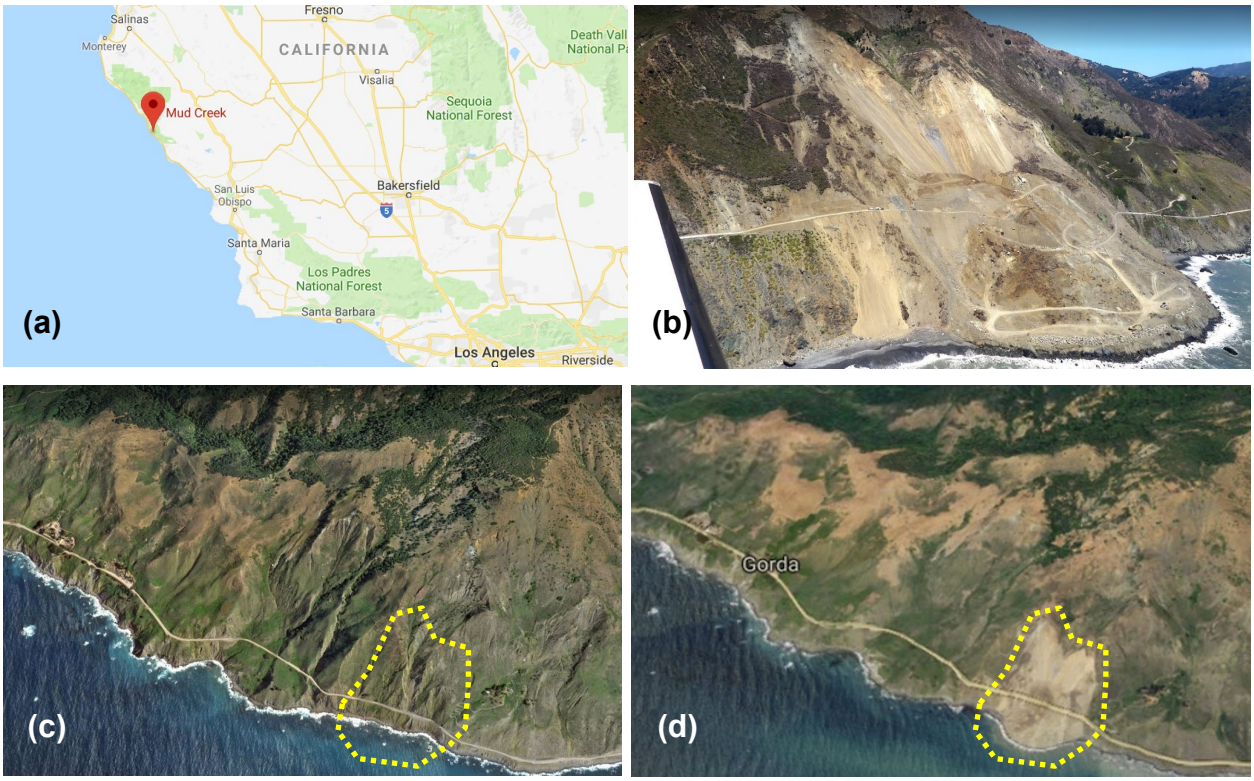

Figure 43: California Highway 1 – Mud Creek landslide: (a) Map; (b) Aerial image of landslide; (c) Satellite imagery before landslide; (d) Satellite imagery after landslide

6.3.1 Test 1 – 2 Weeks before landslide

For this test acquisitions taken on April 25,2017 and May 07,2017 are considered. Figure 44 shows the phase and coherence of the target area. It is evident in the image that there is some phase activity in the slope where the landslide is expected to take place. This

phase activity (highlighted) is different from the phase activity observed when slope instability takes place. This phase activity is most likely attributed to changes in soil moisture content. The coherence is acceptable indicating high signal to noise ratio.

Figure 44: Test 1: (a) Phase map shows disturbances in the area where landslide occurred; (b) Coherence map

6.3.2 Test 2 – 1 Week before landslide

For this test acquisitions taken on May 07,2017 and May 19,2017 are analyzed. Figure 45 shows the phase activity and coherence map. The phase activity is consistent with what was observed in Test 1. The coherence is acceptable indicating high signal to noise ratio.

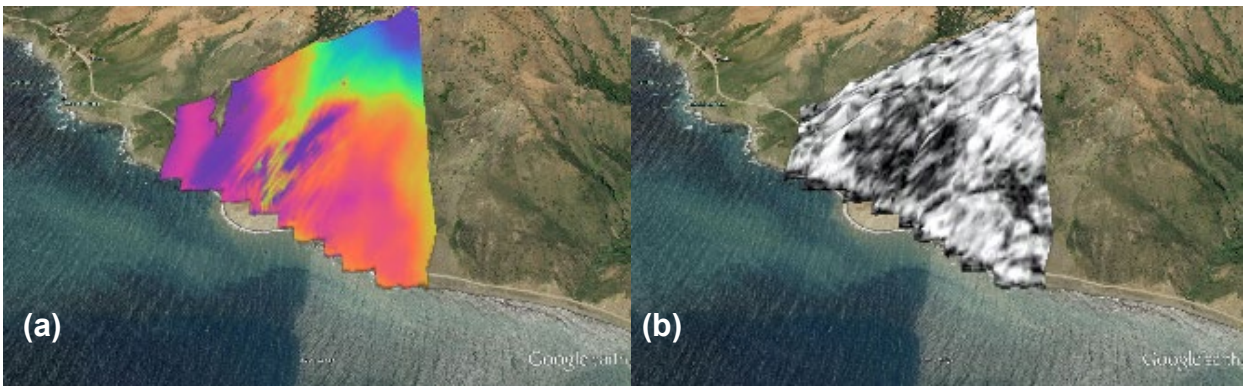

Figure 45: Test 2: (a) Phase map shows disturbances in the area where landslide occurred; (b) Coherence map

6.3.3 Test 3 – Week of landslide

For this test acquisitions taken on May 19,2017 and May 31,2017 are analyzed. It is noted that the landslide occurred on May 20th, 2017. Figure 46 shows the phase and coherence map of the region. In the image, the landslide incident is clearly seen in the phase with the flow pattern covering the area. The coherence however in the area of the landslide is now lower than before.

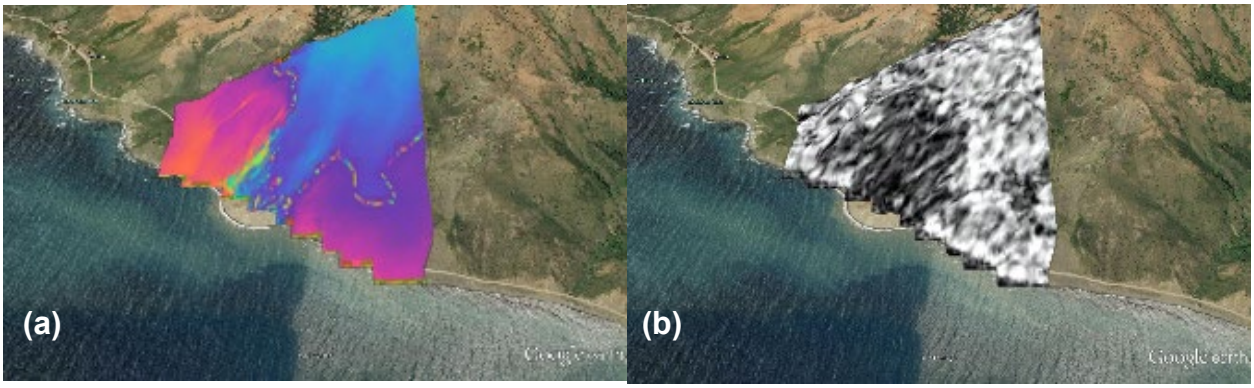

Figure 46: Test 3: (a) Phase map in the area where landslide occurred; (b) Coherence map

6.4 Discussion

The coherence maps of the target region suggest that most of region has good coherence with average coherence being between 0.44 to 0.48 for the 3 cases. The phase map from Test 1 indicates abnormality near the target region. This abnormality is not caused by layering or shadow effect. This can be confirmed from the path of satellite (Ascending). The change in phase can be due to presence of high water content in the soil. News report suggest that the landslide is a type of mudslide and the prominent reason for a mudslide is the water content in soil. This reason is also reinforced by the fact that the radar waves behave differently when they interact with wet and dry soil. The phase map from test 2 also reinforces the observations from test 1. The phase from test 3 which covers the incident shows the landslide taking place. Although displacement maps were not available for this test the phase maps were able to provide a possible landslide recognition opportunity. Further tests must be conducted in similar conditions to confirm these findings.

CHAPTER 7

PSInSAR Showcase Study

This showcase study demonstrates the implementation of the PSInSAR technique to the detection of ground motion in a railway right of way. Similar research is conducted in Europe through the RailSAT program (Samson, 2017). The primary of focus of the RailSAT project is to observe wide area ground deformation rates using Sentinel-1 stacks and focus in urban areas where persistent scatterers are available and easily identified. As compared to RailSAT which seeks to observe deformations in urban settings, the present study observes deformations in more challenging rural settings that lack man-made persistent scatterers, yet is the type of terrain where much of the railway ROW is located.

7.1 Satellite Information

The data for this analysis is acquired by Sentinel-1 of Copernicus satellite constellation. The fist satellite of this constellation Sentinel-1A was launched on 03 April 2014 by European Space Agency. Currently the constellation has 2 satellites (1A and 1B) with 2 more in development. The data is acquired from Sentinel-1A equipped with a C-band radar. The images are acquired in Interferometric Wide (IW) swath mode with each swath being 250km at 5m x 14m spatial resolution. For PSInSAR analysis Single Look Complex (SLC) type of data is used. SLC data is at level 1.1 processing stage which describes the amount of pre-processing the data goes through, the Raw data from the satellite is at level 1.0 and as compared to SLC is unfocused. SLC data contains phase information required for deformation analysis. The images are obtained from Copernicus data hub (ESA, 2018). The 22 SLC images are obtained for the period between August 1st, 2017 and April 10th, 2018 every 12 days. The images are restricted to a single satellite sensor (Sentinel-1A) although data from multiple Satellites over the area are available. This is done to reduce the loss of Persistent Scatterers which occurs when multiple sensors are involve. This test is conducted only in satellite ascending orbit. The test site is located in-between two acquisitions and as such data is unavailable when considering descending orbit satellite.

7.2 Study Site

In this showcase study the Transportation Technology Center (TTC) campus is monitored. “TTCI is a world-class transportation research and testing organization, providing emerging technology solutions for the railway industry throughout North America and the world” (TTCI, 2018). TTC is located in Pueblo, Colorado, and the campus covers an area of 78.12 square miles. It is a subsidiary of Association of American Railroads and operated by Federal Railway Administration (FRA). The center contains 48 miles of railroad track in controlled environment where multiple railway related tests are performed like vehicle stability, safety, endurance, reliability and ride comfort. This area is perfect for this case study as the test performed in this controlled condition can show the scope and limitations of this technique and in-situ measurements exist that can be used for verification studies in future work. Figure 47 shows the location of SAR data covering TTCI.

Figure 47: TTCI Campus - Satellite Image

7.3 Analysis and Results

Displacement maps are the best representation of PSInSAR test results as they indicate the ground subsidence in the direction of satellite Line of Sight. The computed deformations show the subsistence (negative) or rise (positive) at points identified as the persistent scatterers and are in the range -79.8 to 78.5 mm/yr. The results although depicted in mm/year, they represent the total displacement, since the time frame for the analysis is 8 months. Figure 48: Color-coded deformation in mm/yr at the Persistent Scatterers superimposed on Google Earth mapshows the color-coded results at the PS points superimposed on Google Earth for better visualization.

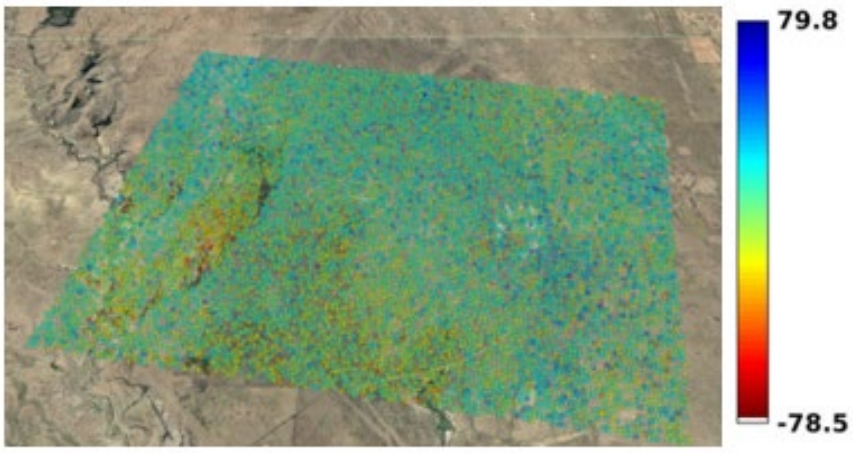

Figure 48: Color-coded deformation in mm/yr at the Persistent Scatterers superimposed on Google Earth map

Figure 49 shows the deformation at the PS points detected in the region near or on the railway track. The PS points are shown as color-coded dots.

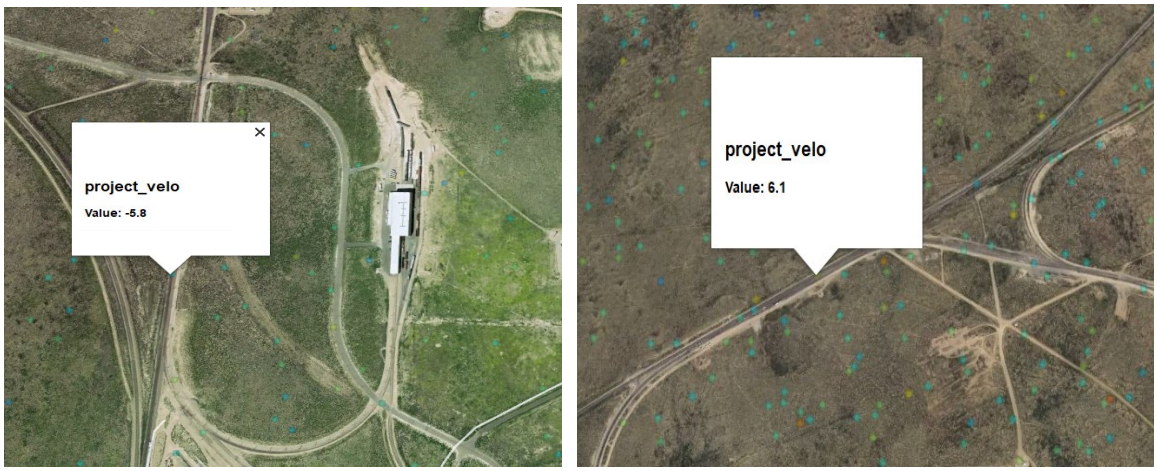

Figure 49: Subsistence at PS identified on the railway track

7.4 Discussion

This case study demonstrated that the PSInSAR technique can be used to compute the deformation at discrete points, the persistent scatteres (PS), using open-sourced satellite data. This analysis has shown that a significantly high number of PS can be detected using this method in a non-urban setting. The results obtained also show that C-band radar is capable of developing images of resolution in mm. It is recommended to verify the accuracy of the measurements in future studies with in-situ readings. The results obtained above show that PSI techniques have good potential in the monitoring of railway Right of Way. Future works should focus on using multiple satellite acquisitions (ascending and descending) to increase the number of PS detected.

CHAPTER 8

Conclusions and Recommendations

InSAR technique has been successfully applied in conjugation with HSR (high-speed railway) in China, Taiwan, and other Asian countries. These techniques have been used to detect instability due to permafrost and groundwater abstraction (Fulong Chen, 2012). In Spain, DInSAR has been used to monitor sinkhole activity. The test has been conducted on two railways stretches. Sinkhole activity was observed in some poorly maintained railroad. From the experiment, the results suggest that the DInSAR method can be used to identify and monitor deformations of railways (J. P. Galve, 2015). It was also suggested the test to be coupled with ground-based measurements. Application of PSA technique to detect land subsidence over HSR has been found to be highly accurate. High precision was available due to high coherent railway lines which greatly helped in the successful application of PSA technique to detect ground subsidence in millimeter range (Yang, 2015).

This work focuses on evaluating the DInSAR and PSInSAR methodologies in analyzing satellite radar images for identifying large- and small- scale ground movements as they related for example to landslides and railroad track subsistence, respectively. The satellite image processing fundamentals and methodologies are investigated and reported. The showcase studies demonstrated that DInSAR can be applied for detecting ground movement. It has also been demonstrated that the DInSAR technique can be applied for detecting changes in the ground moisture, a potential trigger for landslides. At the present development level, only qualitative ground moisture changes and displacements have been conducted. Additional DInSAR studies must be performed in different Line of Sight directions (descending) to get an accurate estimation of landslide activity and improve the displacement maps. The PSInSAR technique has the potential to detect millimeter range variations and can successfully be applied in an urban environment. The technique involves comparing the phase of multiple images and finding persistent scatterers (coherent radar targets). Then using these coherent targets to remove the effect of atmospheric phase components from the rest of the stack. This also helps to remove errors caused by the ionosphere and orbital components. Although the PS technique is more accurate than DInSAR and can remove atmospheric phase most of the time, it has its own disadvantages. The technique requires thirty InSAR images ideally. This can be a drawback when the target has limited SAR coverage. Therefore, PSInSAR cannot replace traditional InSAR yet.

For the development of a monitoring system for the railway right of way it is concluded that:

- The current satellite technology makes it feasible to monitor the railway infrastructure for large- and small-scale deformations and changes in the ground moisture content in adequate resolution.
- The satellite image analysis results can be superimposed to the aerial visual imagery of the target areas for ease of visual inspection and evaluation.
- The frequency of acquisition of satellite images is adequate for the long-term monitoring of the infrastructure.

- Satellite images are available in the public domain.
- Although the computational tasks of this feasibility study were carried out on a desktop and laptop computers, the computing and storage power requirements to conduct such studies can become significant but are not prohibitive.
- The DInSAR technique needs to be expanded to quantify the changes in the ground moisture content.
- The PSInSAR technique needs to be refined to increase the number of detected persistent scatterers.
- Both techniques need to be validated with in-situ measurements through conventional means.

REFERENCES

Agram, P. S., 2013. Principles and theory of radar interferometry - UNAVCO Short Course. [Online]
Available at: https://www.unavco.org/education/professional-development/short-courses/course-materials/insar/2013-insar-roipac-giant-course-materials/InSARPrinciplesTheory_UNAVCO_13_p1.pdf

AIRBUS defence and space, 2014. Terra SAR-X Image product guide, s.l.: s.n.

Alkevli, T. & Ercanoglu, M., 2011. Assessment of ASTER satellite images in landslide inventory mapping: Yenice-Gökçebey (Western Black Sea Region, Turkey). Bulletin of Engineering Geology and the Environment, 70(4), pp. 607-617.

Array Systems, 2017. Synthetic Analysis Tool. [Online]
Available at: http://www.array.ca/solutions/sar-simulation.html

Bianchini, S. et al., 2013. Landslide Activity Maps Generation by Means of Persistent Scatterer Interferometry. Remote Sensing, 5(12), pp. 6198-6222.

Bitelli, G., Dubbini, M. & Zanutta, A., 2004. Terrestrial laser scanning and digital photogrammetry techniques to monitor landslide bodies. International Archives of Photogrammetry, Remote Sensing and Spatial Information Sciences, 35(B5), pp. 246-251.

Blaschke, T., 2010. Object based image analysis for remote sensing. ISPRS Journal of Photogrammetry and Remote Sensing, 65(1), pp. 2-10.

Brockmann Consult, 2017. SNAP. [Online]
Available at: http://web.brockmann-consult.de/portfolio/earth-scientific-image-processing/

Brückl, E., Brunner, F. K. & Kraus, K., 2006. Kinematics of a deep-seated landslide derived from photogrammetric, GPS and geophysical data. Engineering Geology, 88(3), pp. 149-159.

Carl, W., 1951. Synthetic Aperture Radars. IEEE.

Cascini, L. et al., 2010. A new approach to the use of DInSAR data to study slow-moving landslides over large areas. Frascati, FRINGE 2009 Workshop.

Chen, C. W. & Zebker, H. A., 2002. Phase unwrapping for large SAR interferograms: Statistical segmentation and generalized network models. IEEE Transactions on Geoscience and Remote Sensing, Volume 40, pp. 1709-1719.

Chen, W. et al., 2014. Forested landslide detection using LiDAR data and the random forest algorithm: A case study of the Three Gorges, China. Remote Sensing of Environment, Volume 152, pp. 291-301.

Corsini, A. et al., 2009. Coupling geomorphic field observation and LIDAR derivatives to map complex landslides. s.l., Landslides processes—from geomorphologic mapping to dynamic modeling, proceedings of the landslide processes conference.

Costantini, M., 1998. A Novel Phase Unwrapping Method. IEEE TRANSACTIONS ON GEOSCIENCE AND REMOTE SENSING.

CRISP, 2017. Interpreting Optical Remote Sensing Images. [Online]
Available at: https://crisp.nus.edu.sg/~research/tutorial/opt_int.htm

Crosetto, M. et al., 2016. Persistent Scatterer Interferometry: A review. ISPRS Journal of Photogrammetry and Remote Sensing, Volume 115, pp. 78-89.

Dai, F., Lee, C. & Ngai, Y., 2002. Landslide risk assessment and management: an overview. Engineering Geology, Volume 64, pp. 65-87.

Delacourt, C., Allemand, P., Casson, B. & Vadon, H., 2004. Velocity field of the ''La Clapie`re'' landslide measured by thecorrelation of aerial and QuickBird satellite images. Geomphysical Resarch Letters, Volume 31, pp. L15619-L15624.

Delacourt, C. et al., 2009. Observation of a Large Landslide on La Reunion Island Using Differential Sar Interferometry (JERS and Radarsat) and Correlation of Optical (Spot5 and Aerial) Images. Sensors, 9(1), pp. 616-630.

Embury-Dennis, T., 2018. Barcelona train crash: At least one dead and dozens injured as landslide causes derailment in Spain. [Online]
Available at: https://www.independent.co.uk/news/world/europe/barcelona-train-crash-accident-terrassa-manresa-spain-catalonia-landslide-victims-a8642341.html

ESA, 2016. Sentinel-1 overview. [Online]
Available at: https://earth.esa.int/web/sentinel/user-guides/sentinel-1-sar/overview

ESA, 2017. naming conventions. [Online]
Available at: https://earth.esa.int/web/sentinel/user-guides/sentinel-1-sar/naming-conventions

ESA, 2018. Copernicus Open Access Hub. [Online]
Available at: https://scihub.copernicus.eu/

ESA, 2018. SNAPHU. [Online]
Available at: http://step.esa.int/main/third-party-plugins-2/snaphu/
[Accessed 12 2018].

Fantz, A. & Capelouto, S., 2015. Amtrak passenger train derails in Vermont; 6 riders injured. [Online]
Available at: https://edition.cnn.com/2015/10/05/us/vermont-train-derailment/index.html

Ferretti, A., 2014. Satellite InSAR Data Reservoir Monitoring from space. s.l.:EAGE Publications.

Ferretti, A. et al., 2007. InSAR Principles: Guidelines for SAR Interferometry Processing and Interpretation. s.l.:ESA Publications.

Ferretti, A., Prati, C. & Rocca, F., 2000. Nonlinear subsidence rate estimation using permanent scatterers in differential SAR interferometry. IEEE Transactions on Geoscience and Remote Sensing, 38(5), pp. 2202-2212.

Fielding, E. J., 2016. Principles and theory of radar interferometry - UNAVCO Short Course. [Online]
Available at: https://www.unavco.org/education/professional-development/short-courses/course-materials/insar/2016-insar-isce-giant-course-materials/InSARPrinciplesTheory_UNAVCO_2016new.pdf
[Accessed 5 12 2018].

Fiorucci, F. et al., 2011. Seasonal landslide mapping and estimation of landslide mobilization rates using aerial and satellite images. Geomorphology, 129(1-2), pp. 59-70.

Fulong Chen, H. L. Z. L. Q. C. J. Z., 2012. Interaction between permafrost and infrastructure along the Qinghai–Tibet Railway detected via jointly analysis of C- and L-band small baseline SAR interferometry. Remote sensing of Environment, pp. 532-540.

Gillespie, A. R., Kahle, A. B. & Walker, R. E., 1987. Color enhancement of highly correlated images—channel ratio and 'chromaticity' transformation techniques. Remote Sensing of Environment, 22(3), pp. 343-365.

GIM International, 2017. satellite radar interferometry. [Online]
Available at: https://www.gim-international.com/content/article/satellite-radar-interferometry

GISGeography, 2017. A complete guide to LiDAR:light detection and Ranging. [Online]
Available at: http://gisgeography.com/lidar-light-detection-and-ranging/

Goldstein, R. M. ,. W. C. L., 1998. Radar interferogram filtering for geophysical applications. Geophysical Research Letters.

Guarnieri, F. D. Z. a. A. M., 2006. TOPSAR: Terrain Observation by Progressive Scans. IEEE Transactions on Geoscience and Remote Sensing, pp. 2352-2360.

Haeberlin, Y., Turberg, P., Retiere-Senegas, O. & Parriaux, A., 2004. Validation of SPOT-5 satellite imagery for geological hazard identification and risk assessment for landslides, mud and debris flow in Matagalpa, Nicaragua. Istanbul, XXth ISPRS Congress.

Hooper, A., 2008. A multi-temporal InSAR method incorporating both persistent scatterer and small baseline approaches. Geophysical Research Letters, Volume 35, pp. L16,302.

Hooper, A., 2009. StaMPS/MTI Manual. s.l.:Delft Institute of Earth Observation and Space Systems.

Hooper, A. & Zebker, H., 2007. Phase unwrapping in three dimensions with application to InSAR time. Journal os Optical Society of America, Volume 24, pp. 2737-2747.

Hooper, A., Zebker, H., Segall, P. & Kampes, B., 2004. A new method for measuring deformation on volcanoes and other natural terrains using InSAR persistent scatterers. Geophysical Research Letters, 31(23).

J. P. Galve, C. a. F., 2015. Railway deformation detected by DInSAR over active sinkholes in the Ebro Valley evaporite karst, Spain. Natural Hazards and Earth System Science.

Jaboyedoff, M. et al., 2012. Use of LIDAR in landslide investigations: a review. Natural Hazards, 61(1), pp. 5-28.

Kasai, M., Ikeda, M., Toshihiro, A. & Fujisawa, K., 2009. LiDAR-derived DEM evaluation of deep-seated landslides in a steep and rocky region of Japan. Geomorphology, 113(1), pp. 57-69.

Lacroix, P., Zavala, B., Berthier, E. & Audin, L., 2013. Supervised Method of Landslide Inventory Using Panchromatic SPOT5 Images and Application to the Earthquake-Triggered Landslides of Pisco (Peru, 2007, Mw8.0). Remote Sensing , 5(6), pp. 2590-2616.

Lillesand, T. M. & Kiefer, R. W., 2008. Remote sensing and image interpretation. 6th ed. s.l.:John Wiley & Sons.

Liu, J. G., 2000. Smoothing filter based intensity modulation: a spectral preserve image fusion technique for improving spatial details. International Journal of Remote Sensing, 21(18), p. 3461–3472.

Liu, J. G., 2000. Smoothing filter based intensity modulation: a spectral preserve image fusion technique for improving spatial details. International Journal of Remote Sensing, 21(18), p. 3461–3472.

Lu, P., Stumpf, A., Kerle, N. & Casagli, N., 2011. Object-Oriented Change Detection for Landslide Rapid Mapping. IEEE Geoscience and Remote Sensing Letters (GRSL), 8(4), pp. 701-705.

Marcellino, E. V., Formaggio, A. R. & Maeda, E. E., 2009. Landslide inventory using image fusion techniques in Brazil. International Journal of Applied Earth Observation and Geoinformation, 11(3), pp. 181-191.

Massonnet, D. & Adragna, F., 1990. Synthetic Aperture Radar : New Processing Concepts. s.l., IEEE Xplore.

Mathew, P., 1999. Computer Processing of Remotely Sensed Images. New York: John Wiley and Sons.

Mazzanti, P. et al., 2015. Terrestrial SAR Interferometry Monitoring of Natural slopes and Man made structures. s.l., Springer, pp. 189-192.

Moine, M, Puissant, A. & Malet, J. P., 2009. Detection of landslides from aerial and satellite images with a semi-automatic method. Application to the Barcelonnette basin (Alpes-de-Hautes-Provence, France). Strasbourg, s.n., pp. 63-68.

Munzer, j. a. C., 2010. Automatic archaeological feature extraction from satellite VHR images. ACT Astronautica, pp. 1302-1310.

Murillo-Garcia, F. G. et al., 2015. Satellite stereoscopic pair images of very high resolution: a step forward for the development of landslide inventories. Landslides, 12(2), pp. 277-291.

Nichol, J. & Wong, M. S., 2005. Satellite remote sensing for detailed landslide inventories using change detection and image fusion. International Journal of Remote Sensing, 26(9), pp. 1913-1926.

Pamela, E. C. a. M. L. R., 2009. Remote Sensing Tools for Exploration. s.l.:Springer.

Pittsburgh Post Gazette, 2014. [Online]
Available at: http://www.post-gazette.com/local/city/2014/04/08/Landslide-blocks-railroad-tracks-closes-Duquesne-Incline/stories/201404080148

Richards, J., 2009. Remote Sensing with Imaging Radar. s.l.:Springer.

Riedel, B. & Walther, A., 2008. InSAR processing for the recognition of landslides. Advanced Geosciences, Volume 14, pp. 189-194.

Samson, H., 2017. RAILSAT - MONITORING RAILWAY TRACK GEOMETRY AND ITS SURROUNDINGS. [Online]
Available at: https://business.esa.int/projects/railsat
[Accessed 12 2018].

Scaioni, M., Longoni, L., Melillo, V. & Papini, M., 2014. Remote Sensing for Landslide Investigations: An Overview of Recent Achievements and Perspectives. Remote Sensing.

Spiker, E. C. & Gori, P. L., 2003. USGS National Landslide Hazards Mitigation Strategy - A Framework for Loss Reduction, s.l.: US Geological Survey.

Tarchi, D. et al., 2003. Landslide monitoring by using ground-based SAR interferometry: An example of application to the Tessina landslide in Italy. Engineering Geology, 68(1-2), pp. 15-30.

The Spokesman-Review, 2014. [Online]
Available at: http://www.spokesman.com/stories/2014/nov/28/rock-slide-near-bonners-ferry-shuts-down-bnsf-trac/comments/

Travelletti, J. et al., 2012. Correlation of multi-temporal ground-based optical images for landslide monitoring: Application, potential and limitations. SPRS Journal of Photogrammetry and Remote Sensing, Volume 70, pp. 39-55.

TTCI, 2018. Transportation Technology Center. [Online]
Available at: http://www.aar.com/
[Accessed 12 2018].

UNAVCO, 2015. Synthetic Aperture Radar satellites. [Online]
Available at: https://www.unavco.org/instrumentation/geophysical/imaging/sar-satellites/sar-satellites.html
[Accessed 5 12 2018].

Veci, L., 2016. Sentinel-1 Toolbox TOPS Interferometry Tutorial. [Online].

Weng, Q., 2009. Thermal infrared remote sensing for urban climate and environmental studies: Methods, applications, and trends. ISPRS Journal of Photogrammetry and Remote Sensing, 64(4), pp. 335-344.

Yang, Z., 2015. Monitoring and Predicting Railway Subsidence Using InSAR and Time Series Prediction Techniques, Birmingham: The University of Birmingham.

Zhang, Y., 2002. Problems in the fusion of commercial high-resolution satellite as well as Landsat 7 images and initial solutions. Ottawa, s.n.

APPENDICES

Appendix A - Glossary

TOPSAR: TOPSAR is Terrain Observation with Progressive Scans SAR is an acquisition technique. Where data is acquired in long burst by scanning continuously throughout the acquisition from backward to forward. This technique is superior to ScanSAR because this technique is capable of generating homogeneous image quality and same signal-to-noise ratio throughout the swath. This technique causes worsening of azimuth resolution as it concentrates on range coverage to resolution (Guarnieri, 2006).

Coregistration: Coregistration is critical step in which the SAR images from two different acquisitions are aligned. This step is needed to accurately measure phase difference and to reduce noise in the image.

Computation of Interferogram: The process of creating an Interferogram involves the subtraction of flat-earth phase. Flat-earth phase is estimated using the orbital and metadata information. The flat-earth phase is the phase present in the signal (P) due to curvature of reference surface.

TOPS Deburst: Each sub-swath in the acquisition consists of number of bursts. Each burst behaves like a separate SLC (Single look Complex) image. These bursts are separated by demarcation zones that may contain garbage values. The process of removing these demarcation zones and making all burst data in to single product is called Debursting.

TOPS Merging: Each acquisition consists of 3-5 sub-swath based on type of product (3 for IW and 5 for EW). When processing, the sub-swath is chosen depending on target area. Sometimes the target area can lie in between 2 sub-swaths. The process of merging these two sub-swaths to obtain a single product for further analysis is called TOPS Merging

Goldstein Phase Filtering: The quality of the interferogram map is improved by filtering noise. The Goldstein phase filtering method is used to improve the sharpness of the image before the phase unwrapping stage to improve the results in the phase unwrapping process.

Phase Unwrapping: Phase unwrapping is the process of recovering absolute phase data from an array of phase values known only modulo 2 rad. This process is performed in SNAPHU which produces completely unwrapped results which can be used for deformation analysis.

SRTM: Shuttle Radar Topography Mission are DEM developed by radar systems on board the space shuttle Endeavour. This type of DEM is used as reference DEM models for DInSAR analysis. They have been released to public on September 23,2014 by United States Government.

MCF: Minimum Cost Flow Algorithm is a phase unwrapping technique better explained in (Costantini, 1998)

Range Doppler Correction: Range Doppler Terrain Correction is an orthorectification method for geocoding SAR images. It uses available orbit state vector information from metadata and other parameters like radar timing annotations with reference to DEM data to derive precise geolocation information.

Perpendicular Baseline: The distance between two acquisition spots perpendicular to the satellite viewing direction is known as the 'perpendicular baseline'. The smaller the perpendicular baseline the accurate the analysis is going to be (GIM International, 2017).

Polarization: Polarization corresponds to the direction in which radar waves are transmitted and received. Depending on the polarization the results of the experiment can change significantly. Sentinel-1 has 4 level of polarization complexity i.e. it can transmit and receive signals in all polarizations.

DEM: Digital Elevation Model is a digital representation of the terrain surface in 3-D.